

Functional Polymers for Silicon Anodes from Liquid to Solid Electrolyte Batteries

Xiuxia Zuo and Felix H. Richter*

Due to its high theoretical capacity of 3579 mAh g⁻¹, silicon has emerged as a promising next-generation anode material for high-capacity lithium-ion batteries, aiming to meet the growing demand for high energy density electrochemical energy storage devices. However, challenges such as a 280% volume increase during lithiation, low electronic and ionic conductivities, and unstable solid electrolyte interphase severely hinder its practical implementation. Polymers, with their versatility and tailored properties, play a crucial role in addressing these challenges,

although their use varies considerably depending on the type of electrolyte used in the battery. This review categorizes selected polymers into three parts based on their function and use location in batteries with a silicon anode: polymer binders, polymer modifiers, and polymer electrolytes. The physical and chemical properties required for the intended function of the polymers with silicon anodes are explored for liquid, polymer, and solid electrolyte batteries. Promising future research directions for silicon anodes combined with polymers are also highlighted.

1. Introduction

Driven by the imperative to establish a low-carbon society, lithium-ion batteries (LIBs) have made significant advances in powering electronics and electric vehicles (EVs). The demands for higher energy and power density as well as safety concerns related to thermal failures caused by the organic liquid electrolyte in commercial LIBs encourage further research. Addressing these challenges requires the development of high-performance electrode materials with high specific capacity and/or high cell voltage, as well as the adoption of thermally stable solid electrolytes to enhance safety. Combining high-performance electrode materials with solid electrolytes hold promise as a solution to both challenges, offering a path toward the next generation of batteries.^[1–4]

Silicon is a promising anode material that features in different size and morphology, as shown in Figure 1. Its advantages are its theoretical specific capacity of 3579 mAh g⁻¹ (based on Li₁₅Si₄),

electrode potential range of about 0.37–0.45 V versus Li⁺/Li, natural abundance, and cost-effectiveness.^[5] It has been explored as 0D silicon nanoparticles (Si-NP) and microparticles (Si-MP); 1D silicon nanowires/nanotubes (Si-NWs/NTs); 2D silicon films (Si-films); and 3D porous (Si-porous), core-shell, or yolk-shell structures.^[6,7] A significant challenge is the substantial volume change of silicon during cycling, which can reach up to 280% for Li₁₅Si₄.^[8] This typically leads to particle cracking and pulverization, conductive network loss, and repeated generation of the solid electrolyte interface (SEI) on fractured surfaces, all of which contribute to low initial Coulomb efficiency (ICE) and capacity decay of silicon anodes.^[9] Furthermore, the low electronic conductivity of silicon (10^{-5} – 10^{-3} S cm⁻¹) and slow lithium diffusion coefficient (10^{-14} – 10^{-13} cm² s⁻¹) hinder accessing the theoretical capacity and rate capability.^[10–13]

In a battery, the electrolyte enables ion transport and electronically separates the electrodes. The type of electrolyte used determines the fundamental properties of a battery system. The electrolytes can be generally classified based on their ion-conduction mechanism into liquid electrolyte (LE), gel electrolyte (GE), plasticized polymer electrolyte (PPE), dry polymer electrolyte (DPE), solid electrolyte (SE), and hybrid electrolyte (HE). This systematic typology was first introduced by Sen and Richter^[14] to uniquely distinguish different electrolyte and battery types: 1) liquid electrolyte battery (LEB) and gel electrolyte battery (GEB), 2) plasticized polymer electrolyte battery (PPEB) and dry polymer electrolyte battery (DPEB), 3) solid electrolyte battery (SEB), and 4) hybrid electrolyte battery (HEB), as shown in Figure 2.^[14] The HEB may be further distinguished in particle-in-matrix and multilayer assemblies. DPEB, PPEB, SEB, and HEB are collectively referred to as solid-state batteries (SSBs). We use the notation system of ^{AAM}XEB^{CAM} to represent battery cells, where AAM is the anode active material; XEB stands for one of LEB, GEB, PPEB, DPEB, SEB, or HEB; and CAM is the cathode active material.

While LIBs fundamentally rely on metallic redox couples for energy storage, they would cease to function without the

X. Zuo, F. H. Richter
Institute of Physical Chemistry
Center for Materials Research
Justus-Liebig-University Giessen
Heinrich-Buff-Ring 17, 35392 Giessen, Germany
E-mail: Felix.H.Richter@phys.Chemie.uni-giessen.de

X. Zuo
School of New Energy
Ningbo University of Technology
No. 201, Fenghua Road, Jiangbei District, Ningbo, Zhejiang 315211,
P. R. China

X. Zuo
Ningbo Institute of Materials Technology and Engineering
Chinese Academy of Sciences
1219 Zhongguan West Road, Zhenhai District, Ningbo, Zhejiang 315201,
P. R. China

 © 2025 The Author(s). *Batteries & Supercaps* published by Wiley-VCH GmbH. This is an open access article under the terms of the Creative Commons Attribution License, which permits use, distribution and reproduction in any medium, provided the original work is properly cited.

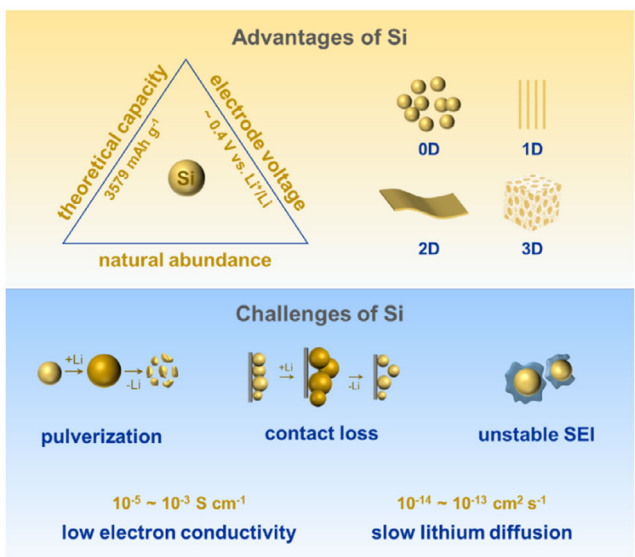


Figure 1. Overview of types of silicon anodes for lithium batteries: advantages and challenges.

contributions of polymeric materials. Polymers play multifaceted roles across battery architectures, serving as binders to maintain electrode integrity, separators to separate cathode and anode, electrolytes facilitating lithium–ion transport, active materials for charge storage, and coatings to suppress interfacial degradation.^[15–18] Focusing on efforts to solve the unique challenges posed by silicon anodes, this review systematically deconstructs three critical functional paradigms of polymers in silicon anode-based batteries: as structural binders, as interface modifiers, and as electrolyte components. The significant 280% volume fluctuation during charging and discharging of silicon poses a formidable challenge, necessitating a suitable design of materials and interface engineering to mitigate contact loss and crack formation. The design of polymer binders, modifiers, and electrolytes requires holistic optimization to unlock the full potential of silicon anodes, leading to significant improvements in battery performance and longevity. In comparison, the investigation of polymers in SSBs with silicon anodes is significantly less developed compared to their widespread adoption in LIBs. This review is conceived to bridge this gap and contribute to advancing the transition from LIBs to SSBs.



Xiu Xia Zuo is currently an associate professor at Ningbo University of Technology (NBUT), China. She received her Ph.D. from the University of Chinese Academy of Sciences in 2018 and subsequently launched her academic career as an associate professor at the Ningbo Institute of Materials Technology and Engineering, Chinese Academy of Sciences. Following 5 years of productive research there, she expanded her expertise through a visiting scholarship in Dr. Felix H. Richter's research group at Justus-Liebig-Universität Gießen, Germany. In 2024, she transitioned to NBUT, where she focuses on designing and developing high-performance anode materials for lithium-ion batteries.

2. Designing Polymers for Silicon Anodes

2.1. Polymer Overview and Properties

Polymers play a critical role in various battery types mentioned above, serving to provide structural support (binders), modify interfaces (modifiers), and enable ionic conduction and electronic insulation (electrolytes).^[19–22] Figure 3 illustrates these three distinct roles in varied locations within batteries, underscoring the necessity for tailored properties based on their function.

Binders are distributed throughout the entire electrode structure, necessitate exceptional binding capability, mechanical integrity, electrochemical stability, solubility and dispersibility, thermal resilience, and eco-friendliness to improve battery performance, longevity, and environmental compliance.^[19,23] Modifiers, integrated solely within or around the active materials, frequently through coating, doping, or compositing, harness properties like structural toughness, flexibility, elasticity, and electronic/ionic conductivity to mitigate contact loss, maintain conductive network, and stabilize the interface between silicon and the electrolyte.^[24,25] As electrolytes, polymers serve as the primary ionic conduction pathway and separator, isolating cathode and anode. These polymers are typically soft, enabling good electrode contact for low interfacial resistance. Important attributes for polymer electrolytes include thermal stability, good mechanical properties, ionic conductivity, electrochemical stability, and high Li⁺ transference number.^[19,20]

To provide an overview, Table 1 classifies a selection of polymers based on their predominant function in silicon electrodes and lists their abbreviations, chemical structures, and properties. It is noteworthy that the same polymer can be applied in different roles, for example, polyaniline can be used both as a binder and as a modifier. The pivotal difference lies in how the polymer is applied, interacts with silicon and acts within the electrode composition. Knowledge of how the polymer functions is essential for optimizing the electrode composition and achieving the desired electrochemical performance of silicon anodes. By carefully selecting and integrating polymers as either binders, modifiers, or electrolytes, the full potential of silicon anodes can be accessed to develop more stable, higher-capacity batteries.



Felix H. Richter is a research group leader in Physical Chemistry at the Center for Materials Research of the Justus-Liebig-University Gießen in Germany. He received a NanoMatFutur research grant from the German Federal Ministry of Education and Research to develop solid-state batteries with polymer protective coatings. The Richter working group focuses on materials innovation, electrochemistry, and characterization in the fields of batteries and ion transport. Concepts that bridge the properties of inorganic materials and polymers are of particular interest to the research efforts of the Richter working group.

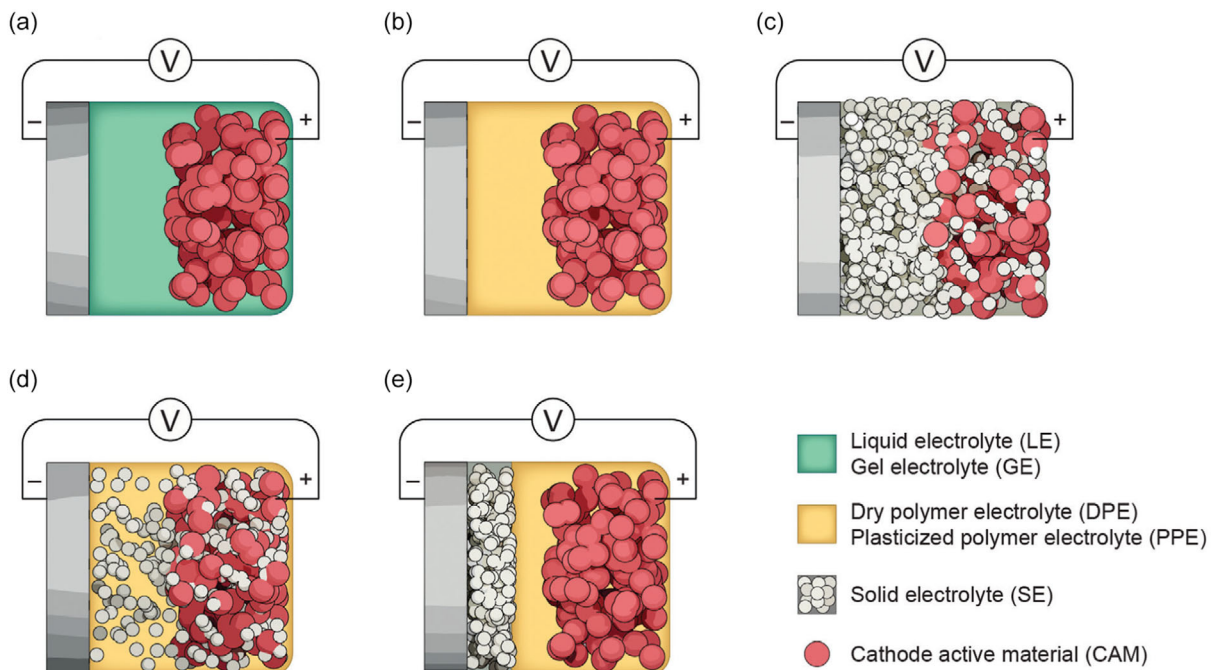


Figure 2. Schematics of batteries made of a metal anode (e.g., lithium), a cathode containing CAM particles and an electrolyte, forming either an a) LEB or GEB, b) DPEB or PPEB, c) SEB, d) particle-in-matrix HEB, or e) multilayer HEB. Reproduced with permission.^[14] Copyright 2023, Wiley-VCH GmbH.

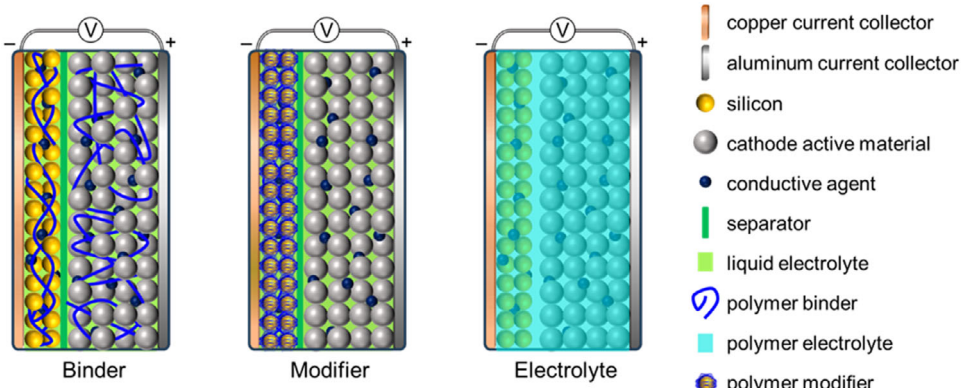


Figure 3. Schematic of the different functions of polymers for batteries with silicon anode: polymer binders, modifiers, and electrolytes.

2.2. Polymer Binders

The rapid development of silicon anodes has driven the role of binders evolving from merely providing mechanical stability to actively influencing battery performance. Novel polymer binders also maintain the electron conductive network and ionic transport at the electrode/electrolyte interface throughout cycling. Moreover, the binder may also act as a buffer to mitigate volume changes and stabilize the SEI.^[26–29] Figure 4 shows schematics of the main functions of polymer binders in silicon anodes, which are discussed individually in the following sections. These functions are achieved by enhancing mechanical interlocking and bonding forces, introducing polar functional groups or reversible bonds, and incorporating conjugated bonds or ionic conductive components. The versatility of polymer structure

and composition enable the development of multifunctional binders tailored to meet the specific requirements of silicon anodes.

2.2.1. Binding Action

The primary function of a binder in electrode construction is to adhere the active material and the conductive additive onto the current collector, ensuring the structural integrity of the electrode throughout the battery life.^[26,30] This adhesion is achieved through two fundamental binding mechanisms: mechanical interlocking and interfacial bonding, as displayed in Figure 4a.^[28]

The mechanical interlocking of binders, influenced by their elasticity, flexibility, and mechanical strength, can be enhanced through copolymerization,^[31,32] crosslinking,^[33–36] grafting,^[37,38]

Table 1. Chemical structures, abbreviations, and properties of polymers used in batteries with silicon anode.

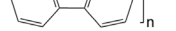
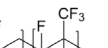
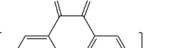
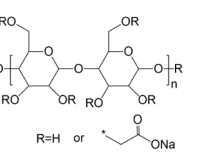
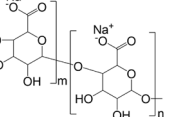
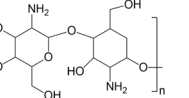
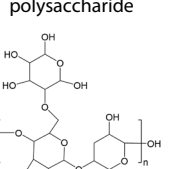
Polymer	Abbreviation	Chemical structure	Properties	Binder	Modifier	Electrolyte
Polymerized styrene butadiene rubber	SBR		High elasticity	[191]	-	-
Polyfluorene	PF		Structural tunability Electronic conductivity (5.5×10^{-2} for cross-linked PF when doped ^[192])	[93–96]	-	-
Poly(1,1-difluoroethylene)	PVDF		High crystallinity High stability Poor elasticity	[56,193–196]	-	[172,174]
Polytetrafluoroethylene	PTFE		Poor adhesion High oxidation stability High thermal stability High elasticity	[31,197]	-	-
Poly (vinylidene fluoride-co-hexafluoropropylene)	P(VDF-co-HFP)		High chemical stability Decent ionic conductivity (with salt) High dielectric constant	-	-	[181]
Polyvinyl alcohol	PVA		Good adhesion	[53,198]	-	-
Polyacrylic acid	PAA		High viscosity Strong hydrogen bonding	[33,40]	-	-
Polyethylene oxide	PEO		High solvating power High mechanical strength Low ionic conductivity Good heat resistance Good adhesion	[99]	-	[167–169,172]
Polyoxadiazole	POD		Good ionic conductivity (with salt) Electronic conductivity (10^{-4} – 10^{-5} S cm ⁻¹ when doped)	[98]	[156]	-
Carboxymethyl cellulose	CMC		High rigidity High brittleness	[44,194]	-	-
Sodium alginate	SA		High viscosity	[45]	-	-
Chitosan	CS		Water soluble Strong hydrogen bonding	[199]	-	-
Gum arabic	GA	polysaccharide	Strong hydrogen bonding	[47]	-	-
Guar gum	GG		High viscosity Good ion conductivity (with salt)	[123]	-	-

Table 1. Continued.

Polymer	Abbreviation	Chemical structure	Properties	Binder	Modifier	Electrolyte
Poly(phenanthrenequinone)	PPQ		Ionic conductivity (with salt) Electronic conductivity (when doped)	[97]	-	-
Polyacrylonitrile	PAN		Good thermal stability Poor mechanical strength	[43,200]	-	-
Polyanilin	PANI		Controllable electronic conductivity (30–200 [80,201] and 400 S·cm⁻¹ [202] when doped) High doping level possible	[81–85]	[112,139–143,152,203]	-
Polypyrrole	PPy		Moderate electronic conductivity (100–7500 [80,201] and 400 [202] S cm⁻¹ when doped) Good thermal stability	[86]	[144–148]	-
Poly(3,4-ethylenedioxythiophene)	PEDOT		High electronic conductivity (300, [202] 1000, [99] 6259 S cm⁻¹ for thin films and 8797 S cm⁻¹ for single crystals [204] when doped) High cycling stability	[100,101]	[100,149–151]	-
Polythiophene	PTh		Good thermal stability Structural tunability Electronic conductivity (10–10³ [80,201] and <10⁻² S cm⁻¹ when doped [99])	[205]	[206]	-

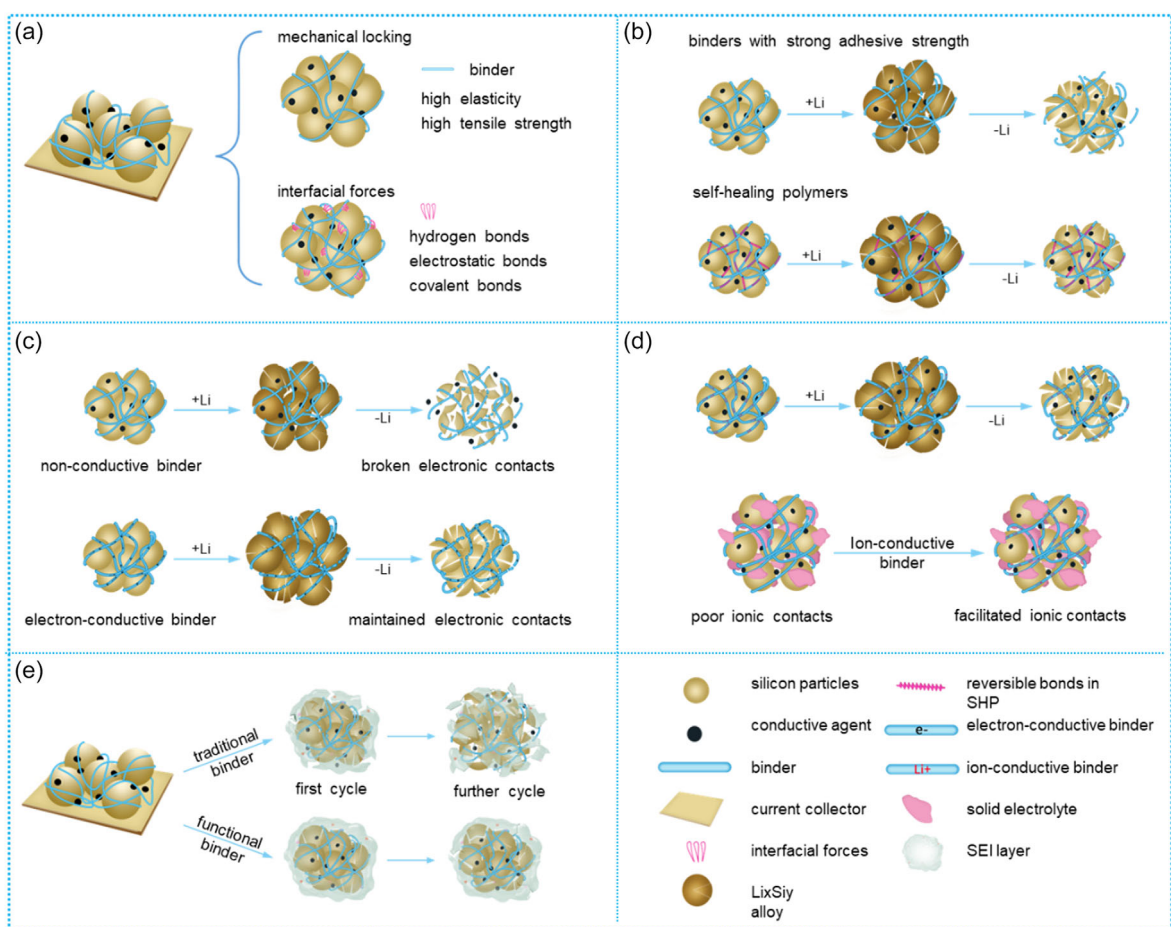


Figure 4. Schematics of the main functions of polymer binders in silicon anodes. a) Polymer binders maintain cohesion of the electrode structure through mechanical interlocking and interfacial bonding. b) Polymer binders with strong adhesive strength or self-healing ability can alleviate the volume expansion of silicon particles. c) Electron-conductive polymers serve as both binders and conductive agents to ensure electronic conductivity and cohesion throughout the electrode. d) Ion-conductive polymers significantly facilitate the ionic transport of the silicon anodes, especially in SSBs. e) Binders containing high-polarity groups or heteroatoms help to form a stable SEI layer on the silicon anode surface.

and incorporation of specific structural elements.^[39] Wang et al. prepared a highly elastic block copolymer PVDF-b-PTFE binder for silicon anodes through block copolymerization of vinylidene fluoride and tetrafluoroethylene. The enhanced elasticity of the obtained polymer network makes it a strong adhesive that adapts to volume fluctuations of silicon anodes, thereby improving the cycling stability, as shown in Figure 5a. It is worth noting that achieving simultaneously mechanical strength and flexibility in

polymer binders is challenging. The structural stability of the silicon electrode during volume changes hinges on both the binder flexibility and strength, necessitating consideration of both factors during binder design.

The interfacial interaction between binders and silicon particles can be enhanced by forming strong hydrogen bonds or covalent bonds through incorporating polar functional groups into polymer structures. Polymers including PAA,^[40,41] PVA,^[42]

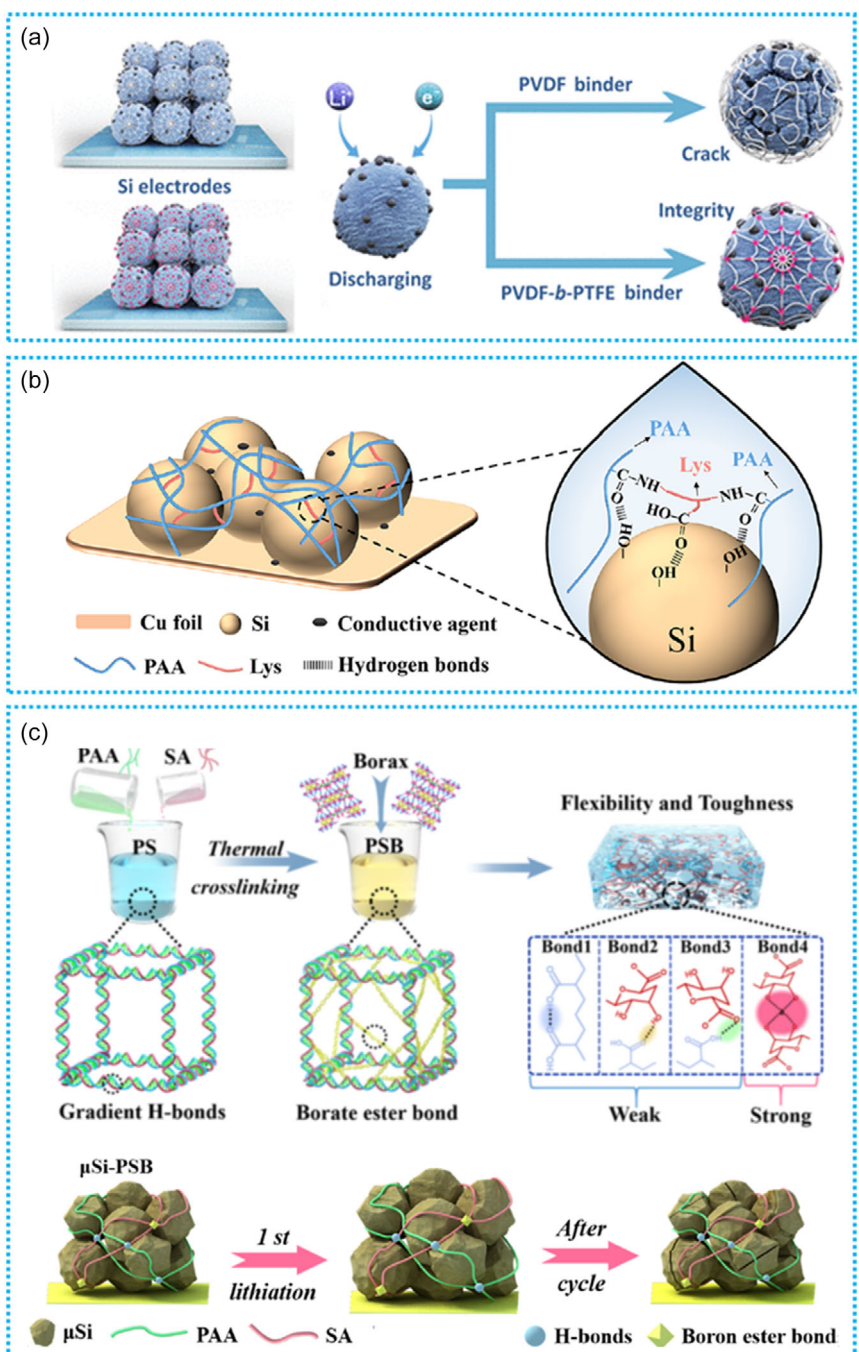


Figure 5. Schematic overview of typical strategies to enhance binding action in silicon anodes. a) Mechanical interlocking: elastic block copolymer PVDF-b-PTFE stabilizing silicon electrodes during electrochemical reactions. Reproduced with permission.^[31] Copyright 2020, American Chemical Society. b) Interfacial binding force: cross-linked polymer binder PAA/Lys interacting with silicon particles. Reproduced with permission.^[33] Copyright 2023, American Chemical Society. c) Combined approach: hierarchical structured polymer binder PSB and its action mechanism. Reproduced with permission.^[55] Copyright 2024, Elsevier.

PAN,^[43] CMC,^[44] SA,^[45] CS,^[46] GA,^[47] GG,^[48] gelatin, as well as their copolymers or composites CS-g-PAA^[49] PVA-g-PAA^[50] PAA-g-SBR,^[51] NaPAA-g-CMC,^[52] and PAA/PVA^[53,54] have become research hotspots due to their abundant hydroxyl and carboxylate functional groups, which can establish robust interfacial binding forces with the silanol groups on the silicon surface. However, before these polymers can adequately adapt to the huge volume change of silicon, especially when the active material loading is increased, there is still considerable room to improve the elasticity and mechanical strength of the binders based on interfacial binding.

Zhang et al. further enhanced the elasticity and adhesion strength of PAA to withstand a strain of up to 400% by cross-linking it with lysine (Lys). The abundance of polar groups in the crosslinked PAA/Lys allows the binder to adhere tightly to silicon particles via hydrogen bonds, as exhibited in Figure 5b. Additionally, the cross-linked structure provides the necessary elasticity to prevent irreversible slipping of the PAA chains upon volume variation of the particles. A $\text{LiLEB}^{\text{Si-NP}}$ using the PAA/Lys binder exhibits a high capacity of 1008 mAh g^{-1} after 250 cycles at 2 A g^{-1} .^[33]

Yan et al. combined intermolecular gradient H-bonds (acting as flexible layers that adapt to volume deformation of microsilicon through stepwise dissociation) with interatomic borate ester bonds (acting as hard layers that proactively alleviate stress concentration, absorb energy, and prevent mechanical fracture of microsilicon during volume expansion) to grant the binder elasticity, toughness, and interfacial bonding force. The binder, designated as PSB, is composed of PAA, SA, and borax. Figure 5c depicts its hierarchical structure, along with an illustration of its action mechanism. The $\text{LiLEB}^{\text{Si-MP}}$ cell utilizing PSB binder demonstrates a high ICE of 93.3% and favorable reversible capacity of 1500 mAh g^{-1} after 600 cycles at 4 A g^{-1} with a capacity retention of 91.4%.^[55]

It is worth noting that the influence of different binders on the performance of silicon anodes in SSBs is significantly lower compared to that in LEBs. Kim et al. conducted a comparative study using PVDF and PAA/CMC as binders and observed that both resulted in similar first-cycle charge capacities and ICE.^[56] That can be attributed to the high stack pressure (140 MPa) applied during the operation of the tested SSBs, which effectively maintains ionic and electronic contacts during cycling of silicon. Therefore, when high pressure is applied, the specific type of binder used for the silicon anode in SSBs appears to be less influential. However, in scenarios where pressure is not applied, the knowledge gained about binders in LEBs remains relevant.

2.2.2. Alleviating Volume Change

As discussed in Section 2.2.1, polymer binders with robust adhesion strength can help to accommodate volume fluctuations of silicon particles and improve their cycling stability. Besides, self-healing polymers (SHPs) with reversible bonds are also very promising in mitigating this issue by spontaneously repairing the mechanical damage and crack at fracture points, thereby creating more stable mechanical and electrical connections among

the silicon particles. Figure 4b demonstrates the advantage of SHPs over traditional binders in mitigating the volume change of silicon particles.^[57]

Hydrogen-bond-directed SHPs are one of the most important SHPs which are widely studied in silicon anodes.^[58–63] The self-healing capability and adhesion strength of SHP binders can be tuned by modifying the cross-linking density, spatial distribution, and segments.^[64–67] Xu et al. developed a PAA-based copolymer binder, poly(acrylic acid)-poly(2-hydroxyethyl acrylate-co-dopamine methacrylate) (PAA-P(HEA-co-DMA)), which forms a multiple self-healing network structure intertwined by hydrogen bonds. This structure stabilizes micron-sized silicon electrodes through a spring expander mechanism, enduring repeated stretching and shrinking cycles without structural degradation, as depicted in Figure 6a. Consequently, even at high areal capacities, the $\text{LiLEB}^{\text{Si-MP}}$ exhibits the reversible capacity of 2394 mAh g^{-1} and 93.8% capacity retention after 220 cycles at 1 A g^{-1} .^[68]

Since hydrogen bonding is relatively susceptible to repeated deformation compared to covalent bonds, there is a growing interest in SHPs that utilize reversible covalent bonds, such as imine bonds,^[69,70] boronated ester bonds,^[71] disulfide bonds,^[72] and Diels–Alder reactions.^[73] Figure 6b demonstrates that a PEG-crosslinked-glycol chitosan polymer (xPEG-GCS) binder, characterized by its reversible imine linkages, possesses the ability to self-heal to its original state when it suffers physical damage. This binder effectively alleviates the volume expansion of a silicon anode, enabling $\text{LiLEB}^{\text{Si-MP}}$ to maintain excellent cycling stability over 1000 cycles.^[69] Figure 6c indicates the incorporation of elastic bifunctional polyurethane (BFPU), featuring disulfide bonds, into PAA binder, which significantly improves the performance of silicon anodes due to the rapid self-healing capability of BFPU and the “hard-to-soft” gradient design.^[72]

In pellet-type SSBs, volume expansion of silicon anodes can be mitigated by the applied external pressure instead of the binder. Reports indicate that proper compressive pressure can cause the formation of numerous perpendicular cracks, which alleviate stress derived from silicon volume variations by repeatedly opening and closing at the same positions, leading to stable cycling performance.^[74,75] However, the relationship between compressive pressure and volume variation in silicon active materials is a complex chemomechanical issue within battery systems, involving not only the anode but also the cathode, SE layer, and other components, necessitating a more comprehensive consideration.^[76–78] In sheet-type SSBs, where the binder is an essential component, the development of multifunctional binders aimed to alleviate volume expansion of silicon anodes is still desirable. In this context, advancements in the aforementioned field of LEBs, particularly in the development of binders with robust adhesion strength and SHP binders, can provide valuable insights and inspiration.

2.2.3. Conducting Electrons

Conventional binders are generally electronically insulating, leading to an increased overall system resistance. Furthermore,

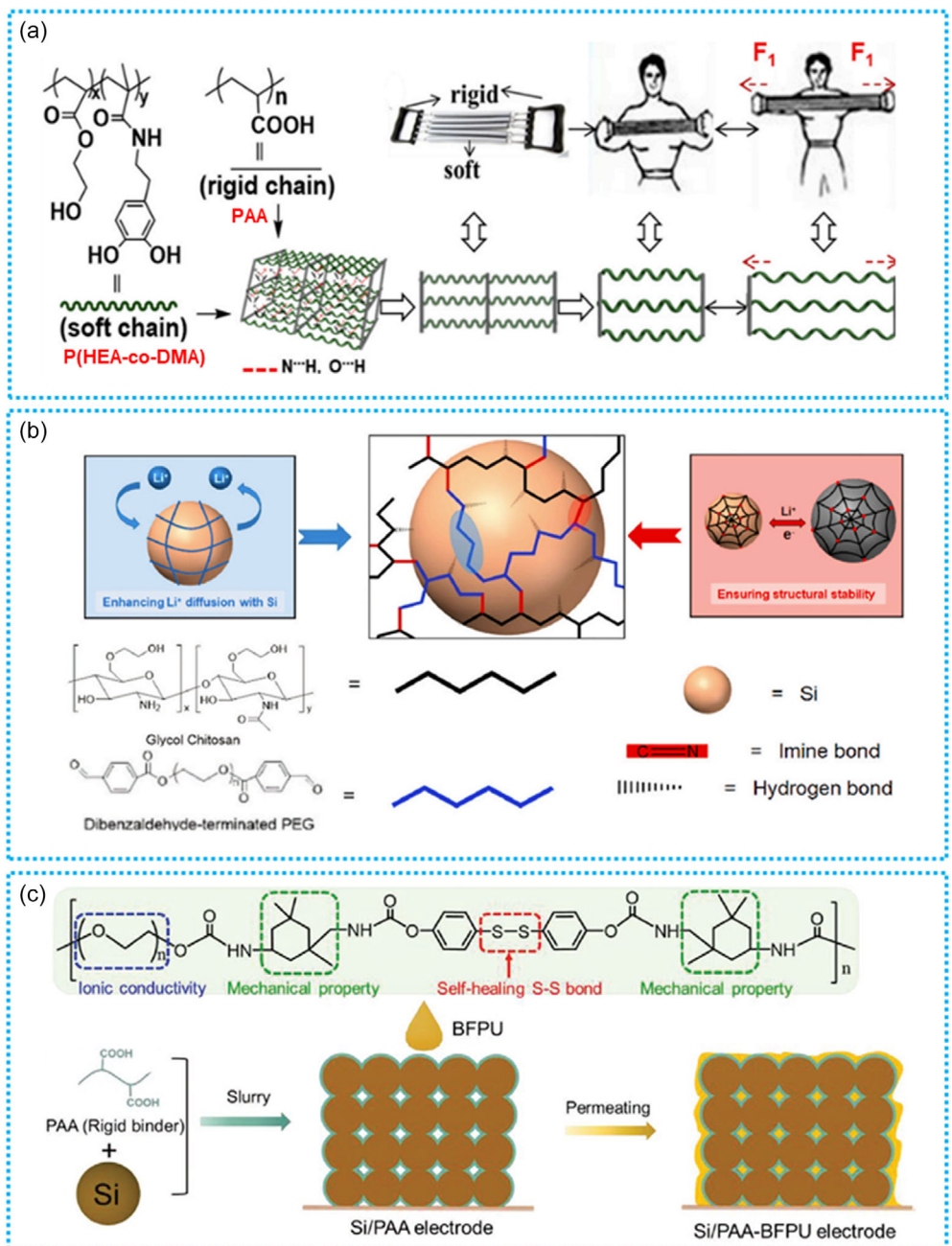


Figure 6. Schematic of strategies to alleviate volume change of silicon anodes through SHP binders featuring a) hydrogen bonds and b,c) covalent bonds. (a) Structure of SHP binder based on spring expanders model, P(HEA-co-DMA). Reproduced with permission.^[68] Copyright 2018, Elsevier. (b) Structure and the adhesion mechanism of the xPEG-GCS binder. Reproduced with permission.^[69] Copyright 2021, Elsevier. (c) Structure of the BFPU polymer and fabrication of the silicon anode with PAA-BFPU binder. Reproduced with permission.^[72] Copyright 2020, Wiley-VCH GmbH.

the electronic pathway facilitated by carbon conductive agents throughout the entire electrode is prone to disruption due to the substantial volume expansion of silicon during lithiation and delithiation. In contrast to nonconductive binders, electron-conductive binders fulfill a dual function, acting as binders and conductive agents.^[28,79] As depicted in Figure 4c, this dual role not only ensures a consistent conductive pathway during volume fluctuations, but also eliminates the need for inactive carbon additives, thereby rendering electron-conductive polymers a research hotspot in the field of binders. The development

of electron-conductive binders mainly revolves around π -conjugated polymers, where electronic conductivity can be regulated through either oxidation (p-doping) or reduction (n-doping).^[80]

The most extensively investigated p-type binders are those based on PANI,^[81–85] PPy,^[86,87] and PEDOT:PSS.^[88–92] However, the p-type conductive polymers do not stay p-doped below a potential of 1 V versus Li⁺/Li, therefore losing electronic conductivity when used in silicon anodes, which are operated between the potential range of 0.01–1 V versus Li⁺/Li. To overcome this limitation, researchers have developed n-type doped polymers

based on PF,^[93–96] PPQ,^[97] and POD^[98] for silicon anodes that exhibit high electronic conductivity in a low potential environment. Despite maintaining the electrode conductivity without the need for additional conducting additives, electron-conductive binders are usually inadequate to preserve the structure integrity of silicon anodes due to their poor mechanical properties and weak adhesion to silicon surface.

To address challenges associated with conductive polymers, various strategies such as crosslinking,^[99–101] chemical coupling,^[91] mixing,^[92,102–105] grafting,^[106] copolymerization,^[107,108] and introducing polar functional groups^[95] have been employed. Zhang

et al. incorporated phytic acid (PA) as both a dopant and cross-linker to form a 3D interconnected conductive network within PANI, as illustrated in Figure 7a. This approach enhances both the electronic conductivity and structural stability of the silicon anode, enabling $\text{LiLEB}^{\text{Si}@\text{SiO}_x}$ cell to achieve a stable reversible capacity of 1137 mAh g^{-1} after 500 cycles at 1 A g^{-1} .^[82]

Kong et al. improved the conductivity, ion diffusivity, and mechanical properties of PEDOT:PSS by mixing it with PEG. The plasticized binder, exhibited in Figure 7b, helps resist silicon anode pulverization during successive lithiation and delithiation cycles and enables a LiLEB^{Si} with a specific capacity of $1871.9 \text{ mAh g}^{-1}$.

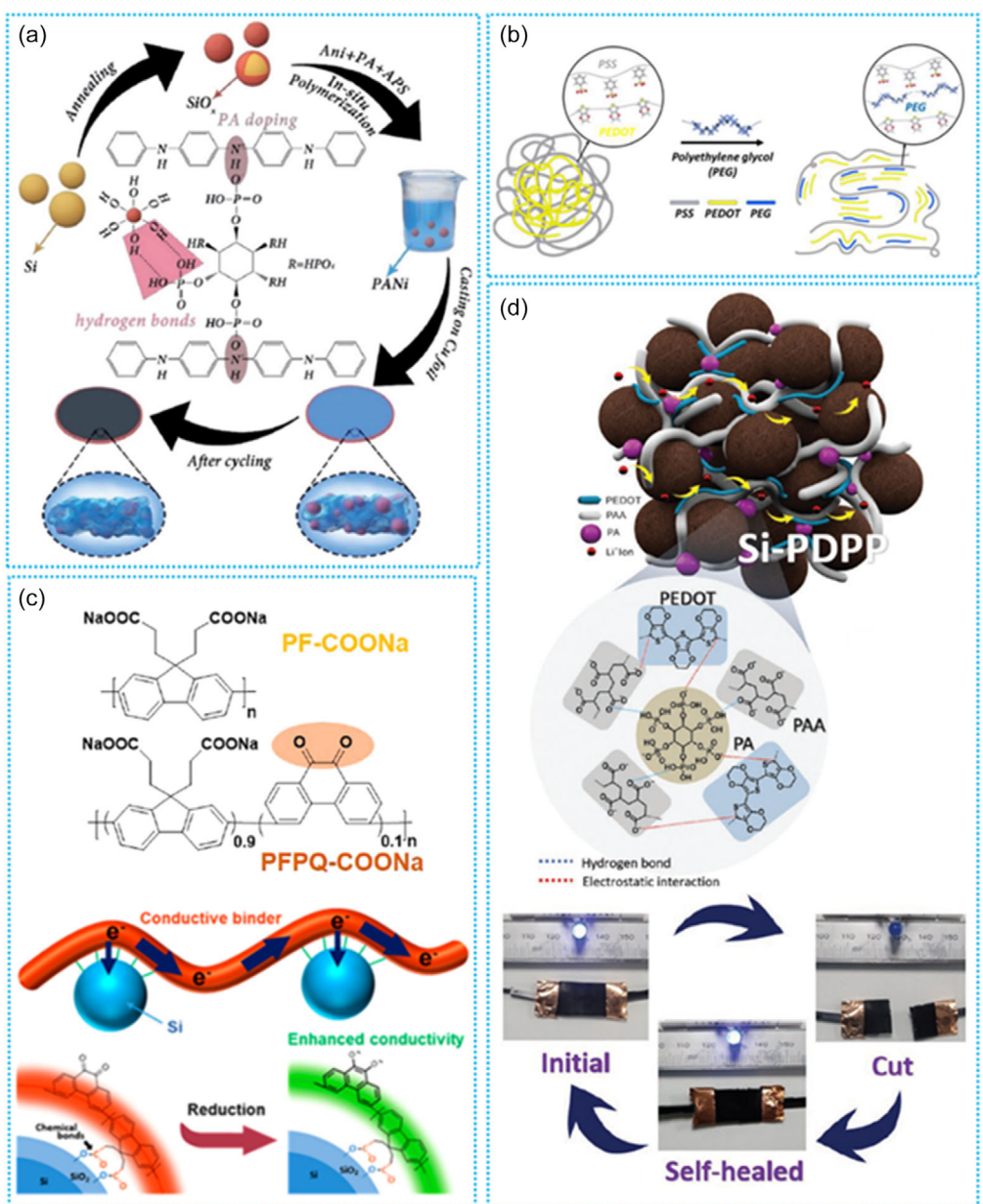


Figure 7. Schematic of strategies to enhance the mechanical properties and interfacial adhesion of conductive polymer binders. a) Crosslinking: crosslinked PANI enhancing the electrode stability of the $\text{Si}@\text{SiO}_x/\text{PANI}$. Reproduced with permission.^[82] Copyright 2020, Royal Society of Chemistry. b) Mixing: mixing with PEG improving the conductivity, ion diffusivity, and mechanical properties of PEDOT:PSS due to plasticizing effect. Reproduced with permission.^[92] Copyright 2024, Elsevier. c) Introducing polar functional groups: introducing PQ enhancing the conductivity of PF-COONa. Reproduced with permission.^[108] Copyright 2018, American Chemical Society. d) Crosslinking: crosslinking PEDOT with PAA endow the conductive binder with self-healing and stretchable properties. Reproduced with permission.^[109] Copyright 2022, Wiley-VCH GmbH.

after 100 cycles at 0.2C.^[92] Pan and colleagues designed a sodium poly(3,3'-(9 H-fluorene-9,9-diyl)dipropionic acid) binder, denoted as PF-COONa, by incorporating carboxyl groups into a PF-based polymer to improve the electronic conductivity and strengthen the bonding force between the conductive polymers and silicon nanoparticles.^[95] They also incorporated 10% phenanthraquinone (PQ) into PF-COONa to further enhance the electronic conductivity by utilizing the carbonyl groups in PQ, which can be reduced to R-O⁻ groups under reductive potential conditions, as shown in Figure 7c. This led to improved cycling stability and rate capability of ^{Li}LEB^{Si} in PFPQ-COONa compared to PF-COONa.^[108]

Malik et al. endowed PEDOT binder with self-healing and stretchable properties by integrating PAA as the primary mechanical support and PA as a multivalent physical crosslinker that facilitates effective interactions between PAA and PEDOT, as shown in Figure 7d. This binder, termed as PDPP, can self-repair the artificially created scratches with a gap width about 10 μm in silicon anodes under practical battery operating conditions, exhibiting a self-healing efficiency of 58% to 82%. A ^{Li}LEB^{Si-NP} using this multifunctional binder achieved an ICE of up to 94% and delivered a reversible capacity of 2312 mAh g⁻¹ after 100 cycles, along with excellent rate capability, providing a capacity of 2084 mAh g⁻¹ at 5C rate.^[109]

Despite efforts to develop electron-conductive polymer binders for silicon anodes in LEBs, few reports exist on their use in SSBs. In a study by Meng and coworkers, PAN was proposed as a precursor to form a partially dehydrogenated and cyclized PAN-based conductive binder in a mesoporous silicon anode for ^{mesop.Si}SEB^{InLi} with thiophosphate-based glass electrolyte.^[110] Dunlap et al. employed a similar PAN-based conducting binder in a ^{Si-NP}SEB^{InLi} cell with silicon-rich (70 wt%) sheet anode and Li₆PS₅Cl electrolyte, achieving high capacities of 1500 mAh g⁻¹ at a 1C rate.^[111] However, the use of conductive polymer binders in SSBs raises concerns about potential decomposition of the SE, leading to increased internal resistance and cell degradation.^[96,112] Given that some conductive agent is still employed in silicon composite anodes, leading to notable performance enhancements, a trade-off emerges between the adverse effects of side reactions with SE and the beneficial effects of conductive networks within the electrode.^[113-116] Thus, with proper consideration, conductive polymer binders still hold potential for application in SSBs with silicon anode.

2.2.4. Conducting Ions

Analogous to electronic conductivity, ionic conductivity is also crucial in governing the kinetics of electrochemical processes. Ion-conductive binders can sustain the continuous ionic pathway throughout the electrode, especially in SSBs, as exhibited in Figure 4d.^[117] Polymers such as chitosan,^[118] starch,^[119,120] PEO,^[121,122] GG,^[123] and Nafion^[124] have been extensively explored as binders to enhance the ionic conductivity of silicon electrodes. Additionally, some of these polymers are also utilized as matrices for polymer electrolytes in the field of SSBs.^[125,126]

The lone pair electrons present in polymer chains can coordinate with solvated lithium ions and promote their transport

through chain segmental motion. Figure 8a provides an illustration of this ionic conduction mechanism of GG binder. Based on this, Zeng et al. developed a binder for silicon anodes by integrating PEO and PEI with PEDOT:PSS through crosslinking and electrostatic interactions, noting that both PEO and PEI possess abundant lone electron pairs, as shown in Figure 8b. This composite polymer binder demonstrated superior lithium-ion and electron transport properties that are 14 and 90 times higher than those of the widely used CMC binder supplemented with acetylene black. The advancement enables ^{Li}LEB^{Si-NP} to achieve a high reversible capacity exceeding 2000 mAh g⁻¹ after 500 cycles at 1 A g⁻¹ while maintaining a capacity of 1500 mAh g⁻¹ at a high current density of 8 A g⁻¹.^[99]

Wan et al. designed a binder by grafting dopamine (DA) onto PAA and mixing it with PVA, where the nitrogen-rich lone pair electrons in DA facilitate the transport of lithium ions through the formation of coordination bonds, as depicted in Figure 8c. Furthermore, the covalent segment of the binder enhances electrode deformation resistance, while the dynamically reversible noncovalent bonds dissipate the expansion/contraction stress within the electrode. Consequently, the ^{Li}LEB^{Si-NP} cell with this PAA-DA/PVA binder retained a capacity of 1974 mAh g⁻¹ after 500 cycles at 4 A g⁻¹.^[127]

In addition to incorporating lone pair electrons, decreasing the crystallinity of polymer binder can also improve the ionic conductivity of silicon anodes due to the enhanced segmental chain motions.^[128] Furthermore, ionization can also facilitate the transport of lithium ions through the lithiated groups of polymers.^[129] Li et al. developed a trifunctional network binder (N-P-LiPN) with hard/soft modulation, employing partially lithiated PAA as the structural backbone and partially lithiated Nafion as the flexible buffer, as exhibited in Figure 8d. This binder increases the ionic conductivity of the silicon anode by facilitating the transfer of lithium ions through its lithiated groups. Furthermore, N-P-LiPN demonstrated robust adhesion and mechanical strength, effectively accommodating the substantial volume changes of the silicon anode. The ^{Li}LEB^{Si-NP} cell with N-P-LiPN as binder achieves an ICE of 93.2% and maintains a discharge capacity of 2143 mAh g⁻¹ after 100 cycles, outperforming cells with nonlithiated binders.^[130]

Different from LEs, SEs are unable to flow around particles and ensure complete access to all active materials, resulting in inadequate ionic conductivity within the electrode of SSBs. Especially, conventional nonconductive binders interrupt the charge transfer pathways within composite electrodes, thereby compromising cell performance.^[131,132] Consequently, the development of ion-conductive binders for SSBs may be crucial. Jung and coworkers revealed that the use of ion-conductive polymer binders significantly enhances the electrochemical performance of ^{InLi}SEB^{NCM} and ^{LTO}SEB^{NCM}, surpassing that achieved with nonconductive NBR binders.^[117] Lee and coworkers employed PAN as precursor to form an electronic and ionic mixed-conducting binder to improve the silicon anode performance in ^{Si-NP}SEB^{InLi} with thiophosphate-based glass electrolyte.^[111] Given the limited research on ionic conductive binders for the performance improvement of silicon anodes in SSBs, this area offers immense prospects for future exploration and development. Both strategies—integrating

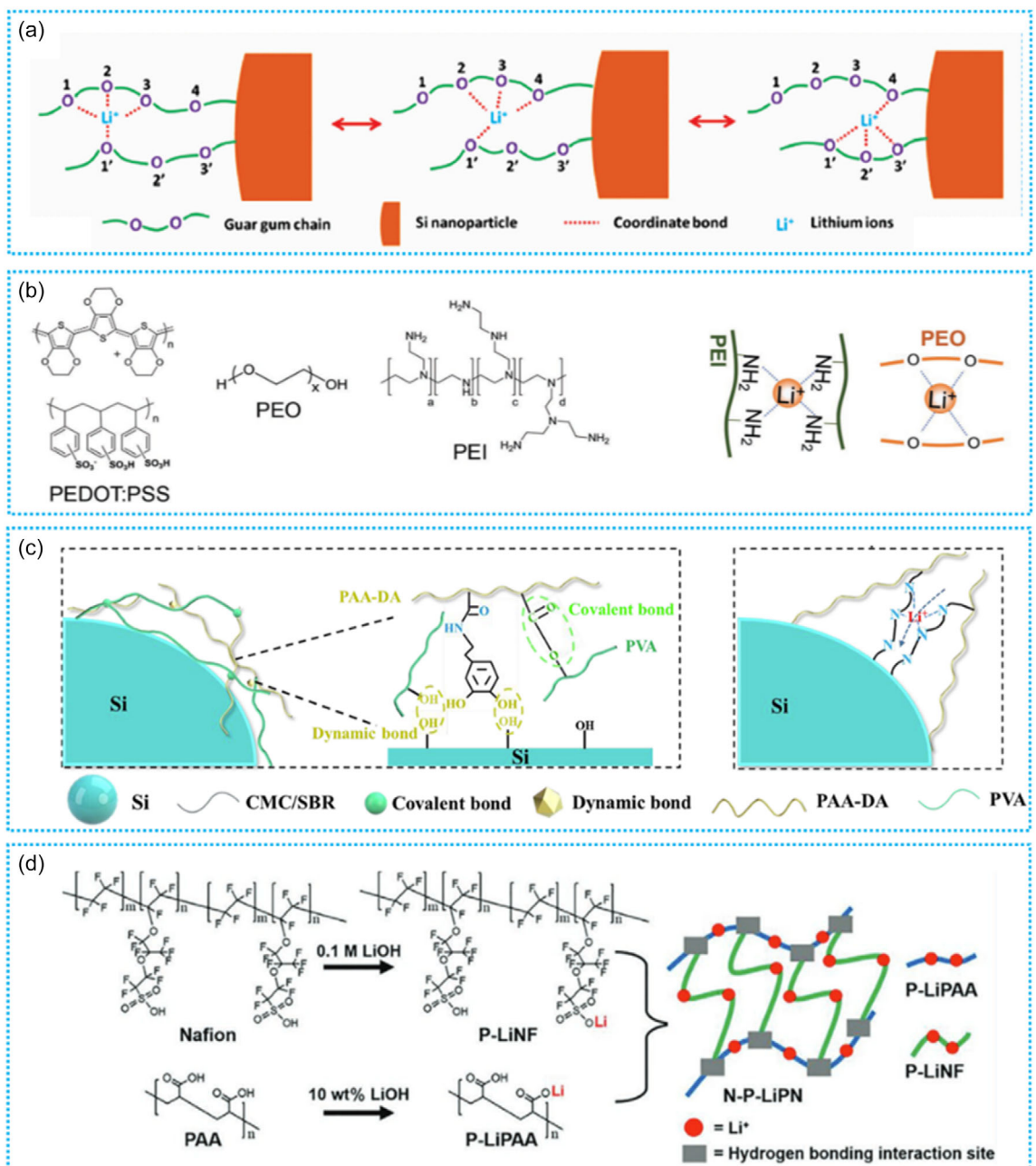


Figure 8. Schematic of strategies to enhance ionic conductivity of polymer binders. a) Incorporating lone pair electrons: oxygen lone pairs in complexation sites facilitating lithium-ion transport with the assistance of segmental motion of the GG binder. Reproduced with permission.^[123] Copyright 2015, Wiley-VCH GmbH. b) Incorporating lone pair electrons: lone electron pairs in PEO and PEI enhancing lithium-ion transport of PEDOT:PSS based binder. Reproduced with permission.^[99] Copyright 2018, Wiley-VCH GmbH. c) Incorporating lone pair electrons: nitrogen-rich lone pair electrons in DA accelerating the lithium ion transport in PAA-DA binder. Reproduced with permission.^[127] Copyright 2022, American Chemical Society. d) Ionization: lithiated N-P-LiPN binder facilitating the transfer of lithium-ions through its lithiated groups. Reproduced with permission.^[130] Copyright 2020, Wiley-VCH GmbH.

polymers with lone pair electrons in the chain and utilizing lithium-ionized polymers—have proven effective in silicon anode-based LEBs and are anticipated to be effective in SSBs as well.

2.2.5. Stabilizing the SEI

The uniform and stable SEI layer can effectively reduce electrolyte consumption and preserve the structural integrity of silicon anodes during repeated volume changes, as shown in Figure 4e. Polymer

binders, such as PAA, PVA, and SA, have been demonstrated to promote the formation of a more stable SEI layer on the silicon surface, thereby enabling better cycling stability of the silicon anodes. The enhancement primarily stems from the interactions between the polar groups in these binders and the lithium salt in the electrolyte, which yields an optimal composition and thickness of the SEI via influencing the formation of different SEI species.^[45,53,133–135] For example, a faster decomposition of FSI^- was observed in the PAA binder-based silicon anode due

to the strong hydrogen bonding with F^- from -COOH group, leading to the formation of LiF within the first few cycles, making F^- unavailable for subsequent SEI formation cycles. This allows further decomposition of the LiFSI salt to sulfates and sulfides, which form a crucial component of the SEI around silicon nanoparticles. In contrast, when using the CMC binder, the weaker intermolecular hydrogen bond strength, arising from the -OH functional group, results in a slower decomposition of LiFSI and the absence of sulfide formation at the initial cycle. Consequently, the dual effects of faster consumption of F^- to form LiF together with the homogeneous distribution of passivating sulfides in the SEI could allow for better capacity retention for silicon anodes in the PAA binder system as compared to that with CMC.^[133]

In poly- γ -glutamate binder, both the oxygen atoms and the nitrogen atoms can serve as a Lewis base to coordinate lithium

ions. This coordination enhances the desolvation of lithium–ions for insertion into Si/graphite anode across the interface. As a result, the Si/graphite anode demonstrates higher electrochemical lithiation reversibility compared to that of polyacrylate and polysaccharides that have no -NH- groups.^[135] Similarly, poly(vinylamine) (PVAm) fosters the formation of a mechanically stable, nitrogen-enriched inorganic SEI that effectively dissipates stress and preserve the structural integrity of silicon anode, as exhibited in Figure 9a.^[136] Furthermore, the electron-deficient boron element, present in boric acid crosslinked PVA binders (Figure 9b), efficiently captures electrons and forms lithium borate species in SEI film, enhancing the mechanical stability of SEI on silicon anodes, thus contributing to an ICE of up to 92.8% and a capacity of $\approx 1884 \text{ mAh g}^{-1}$ after 500 cycles in ${}^{\text{Li}}\text{LEB}^{\text{Si-NP}}$ cells.^[137] Fluorinated binder can be preferentially

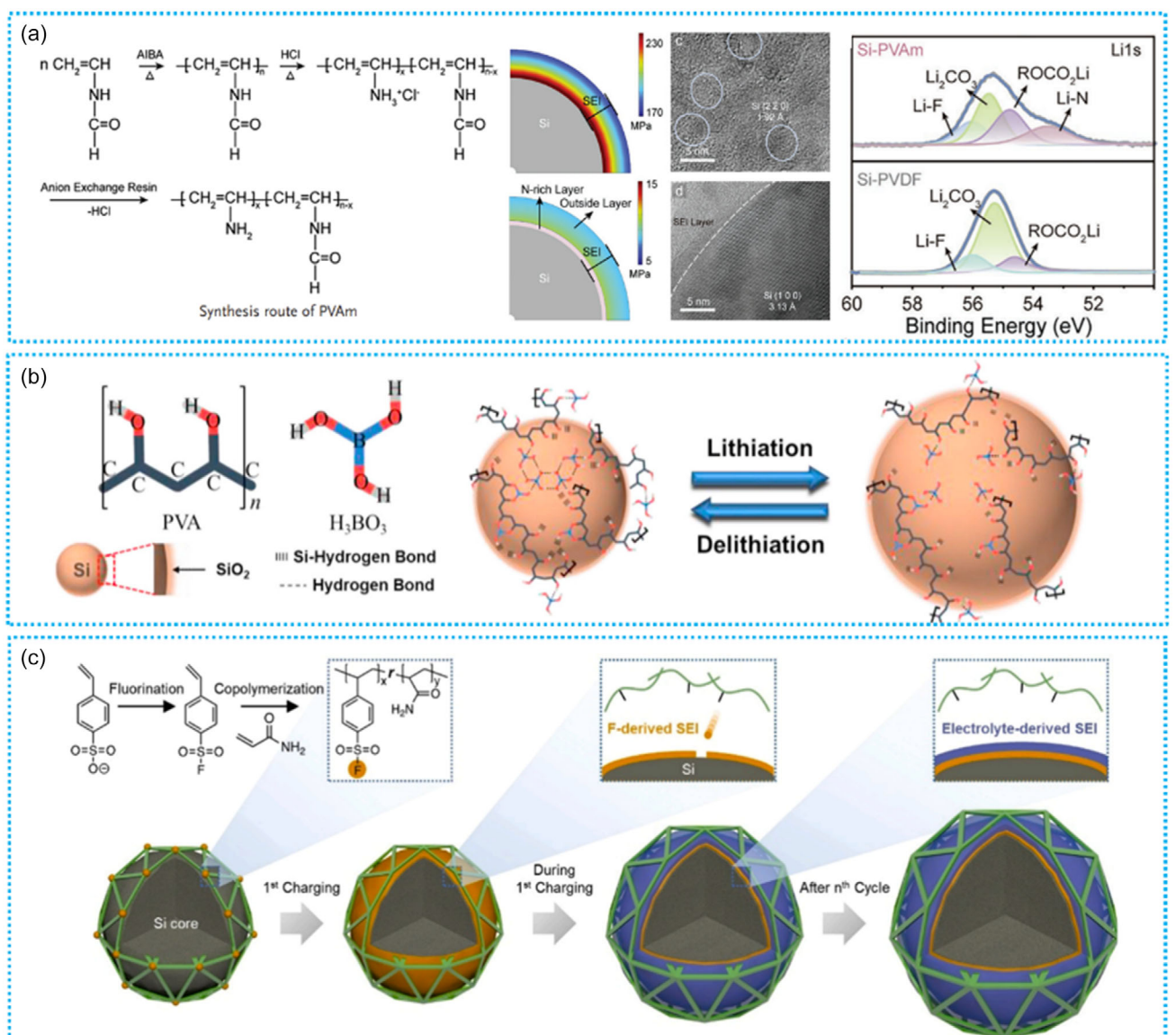


Figure 9. Strategies to construct stable SEI for silicon anodes through incorporating boron, nitrogen, and fluorine elements into binders: a) PVAm binder fostering the formation of a mechanically stable, nitrogen-enriched inorganic SEI. Reproduced with permission.^[136] Copyright 2023, Wiley-VCH GmbH. b) PVA crosslinked by boric acid contributing to an effective SEI film on silicon anode. Reproduced with permission.^[137] Copyright 2020, Elsevier. c) Fluorinated binder facilitating the formation of a stable SEI layer on silicon during the cycle. Reproduced with permission.^[138] Copyright 2024, Elsevier.

reduced at higher voltages compared to traditional electrolytes, leading to the formation of a stable and uniform lithium fluoride (LiF)-based SEI layer on silicon anodes, as illustrated in Figure 9c. The ${}^{\text{Li}}\text{LEB}^{\text{Si-NP}}$ presents a remarkable capacity retention of 93.7% after 400 cycles at 0.9 A g^{-1} .^[138]

These advancements underscore the potential of SEI interface engineering through binders enriched with polar groups or heteroatom elements to enhance the performance of silicon anodes. However, the intricate details of the formation mechanism and growth process of the SEI remain insufficiently elucidated especially in SSBs featuring silicon-based anodes. This holds true regardless of whether it is instigated by electrolyte decomposition or accelerated by carbon additives/binders. The SEI, being the most critical yet least understood aspect of SSBs, necessitates further in-depth studies.^[2]

To summarize, polymer binders exhibit remarkable versatility in silicon anode based LEBs, fulfilling not only the fundamental roles of binding but also significantly alleviating critical issues of silicon anodes, including dramatic volume changes, inadequate Li^+/e^- conductivity, and uncontrollable SEI formation. These diverse functionalities can be achieved through incorporating polar groups, continuous π -conjugated bonds, elements with lone pair electrons, or heteroatomic elements. However, most current binder research focuses on achieving only one or two, or at most three of these functions, with multifunctional binders being rarely reported. Therefore, future research should prioritize the development of multifunctional binders that exhibit good adhesion, self-healing, mixed-conducting properties, and SEI regulation functionality. Achieving this requires a thorough understanding of the mechanisms underlying these functionalities from both macroscopic and microscopic perspectives, as outlined in this manuscript. Innovative polymer design is essential for enabling these functionalities.

In SSBs, binders are exclusively required in sheet-type configurations, where their functions differ from those in LEBs. Given that volume expansion can be mitigated by external pressure, and electronic conductivity may lead to undesirable side reactions with SEs, the primary focus for binder development in SSBs should be on enhancing ionic conductivity and optimizing SEI interface engineering. Strategies employed in LEBs can serve as a reference for these efforts.

2.3. Polymer Modifiers

The versatility of polymers allows them to function not only as binders but also as modifiers. Compositing silicon with polymers proves to be another effective strategy to address the challenges of silicon anodes. In this context, we refer to these polymers as modifiers, emphasizing their role in enhancing the silicon performance as LEB anodes.

The difference of binder and modifier lies in how the polymer integrates with silicon and the resulting electrode composition. Specifically, when serving as a binder, the polymer is usually added during slurry processing, eliminating the need for extra binders in the electrode formulation. In contrast, when employed as a modifier, the polymer must first be composited with silicon

active material before slurry and electrode formation, wherein the inclusion of binders remains essential. Understanding the difference in how the polymer functions as a binder versus a modifier is relevant for optimizing the electrode composition and achieving the desired electrochemical performance of LIBs with silicon anode. By carefully selecting and integrating polymers as modifiers, researchers can harness the full potential of silicon anodes, developing more stable, higher-capacity LIBs.

2.3.1. Electron-Conductive Polymer Modifiers

Limited surface contact between silicon particles and conductive agent as well as the disruption of contact due to the significant volume change of silicon during cycling contributes to rapid capacity fading. Silicon with conductive polymer modifier can keep electrochemically active and achieve stable and reversible cycling. The extensively researched conductive polymer modifiers include PANI,^[112,139–143] PPy,^[144–148] and PEDOT,^[90,100,149–151] which share similarities with electron-conductive binders. Most Si/PANI composites present a core-shell architecture, where the amorphous PANI shell establishes a continuous electronically conductive network while shielding the silicon cores from direct electrolyte exposure. This design mitigates the repeated destruction/reconstruction processes of SEI and improves the structural and cycling stability.

Pan et al. *in situ* coated silicon nanoparticles with a layered conductive PANI, termed LCP, utilizing (trimethoxysilyl) propyl-aniline (TMSPA) as bridge. The LCP layer not only enhances the electronic conductivity of the electrode, but also promotes the formation of an integrated hybrid SEI skin (hSEI). This LCP-integrated hSEI skin exhibits a uniform distribution of inorganic components, which helps homogenize lithium-ion flux and provides flexibility to accommodate dynamic interface changes, as depicted in Figure 10a. Consequently, the resulting ${}^{\text{Li}}\text{LEB}^{\text{Si-NP}}$ delivers a reversible capacity over 1000 mAh g^{-1} after 300 cycles at 1 A g^{-1} , an area capacity of 3 mAh cm^{-2} after 150 cycles at 0.5 mA cm^{-2} , and a higher rate capacity of 942 mAh g^{-1} at 5 A g^{-1} .^[152] In a parallel study, Xu et al. *in situ* synthesized yolk-shell PPy-Fe-coated porous silicon microspheres, showcased in Figure 10b. This approach accelerated charge transfer and ion diffusion while mitigating the structural expansion of silicon, leading to improved cycling and rate capabilities compared to pure silicon.^[148]

Despite these advances, a critical focus should be placed on the polymer modifier ability to maintain conductivity consistently throughout the entire operating potential range of silicon anodes. Any loss of conductivity can trigger polarization in composite electrodes, leading to a decrease in capacity and a subsequent decline in battery lifespan. Furthermore, silicon/polymer composites typically incorporate over 15 wt% of polymer, inherently compromising battery energy density. Despite this substantial proportion, it fails to adequately mitigate the requirement for conductive agents in electrode formulation, emphasizing the urgency to explore and develop more advanced modifiers. While *in situ* polymerization boasts advantages over direct mixing, such as conformal coating and seamless electronic

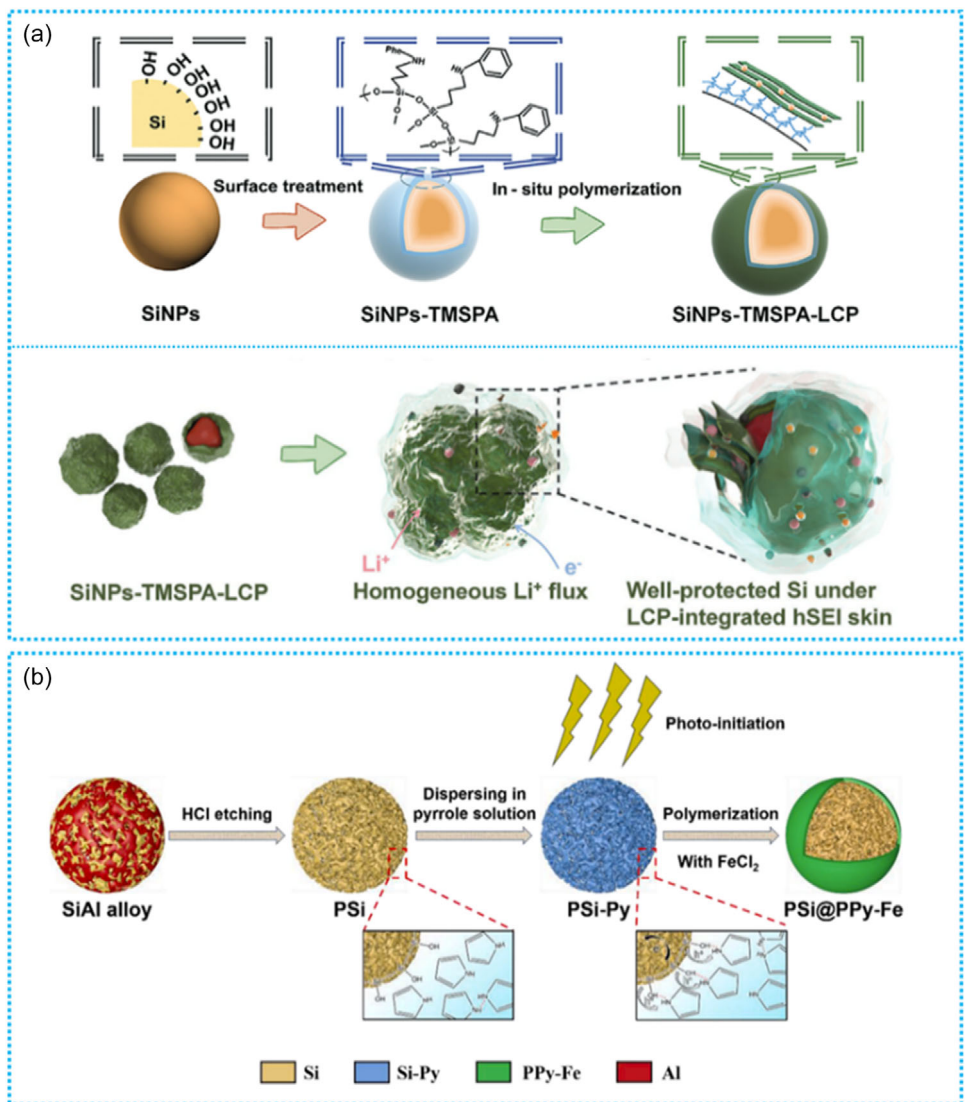


Figure 10. Schematic of two typical silicon and electron-conductive polymer composites. a) Process for fabricating SiNPs-TMSPA-LCP and its evolution of interfacial stability during cycling. Reproduced with permission.^[152] Copyright 2022, Wiley-VCH GmbH. b) Synthetic illustration for photo-initiated in situ synthesis of PSi@PPy-Fe composite. Reproduced with permission.^[148] Copyright 2023, Elsevier.

pathways, its intricate, time-consuming, and complex nature hinders large-scale adoption. Hence, ongoing research should prioritize minimizing modifier content while enhancing conductivity, refining manufacturing processes to maintain conformal coating efficacy while simplifying complexity.

2.3.2. Ion-Conductive Polymer Modifiers

Ion-conductive polymers can also be combined with silicon to enhance the performance, stability, and lifespan of silicon anodes. In a study by Song et al., an enhanced rate capability of silicon was achieved by leveraging the wettability of PAN toward LEs and prioritizing the lithium-ion current flow over electron conduction, as demonstrated in Figure 11a. This strategic approach enables the ^{Li}LEB^{Si-NP@PAN} to retain 62% of its 0.2C rate discharge capacity at an exceptional rate of 10°C.^[153] Crosslinked PAN outperforms linear PAN in enhancing the performance of Si-NPs as it retains its elastic integrity even after absorbing polar LE.^[154]

Delving deeper, the interaction between polymer and electrolyte is a crucial determinant of the ionic conductivity within polymeric materials. Polyparaphenylene (PPP) exhibits a reversible n-doping/de-doping processes within the electrolyte, thereby promoting lithium-ion transfer between the electrolyte and active silicon electrode and improving cycling stability.^[155] Poly(hexaazatrinaphthalene) (PHATN), endowed with $-C=N-$ groups in its benzene rings, accepts lithium ions from the electrolyte, thereby facilitating the construction of robust lithium-enriched surface coatings on silicon, as illustrated in Figure 11b.^[25]

Biphenyl-polyoxadiazole (bPOD) presents abundant sulfonation groups as well as sp^2 hybrid lone pair electrons emanating from nitrogen atoms on its oxadiazole ring, which collectively contribute to a highly conductive environment for ion and electron transport, as displayed in Figure 11c.^[156] LiPAA provides transport sites for lithium ions and acts as surface passivation layers to inhibit electrolyte decomposition and prevent capacity fade.^[157] Based on the lithium-ion conductive mechanism

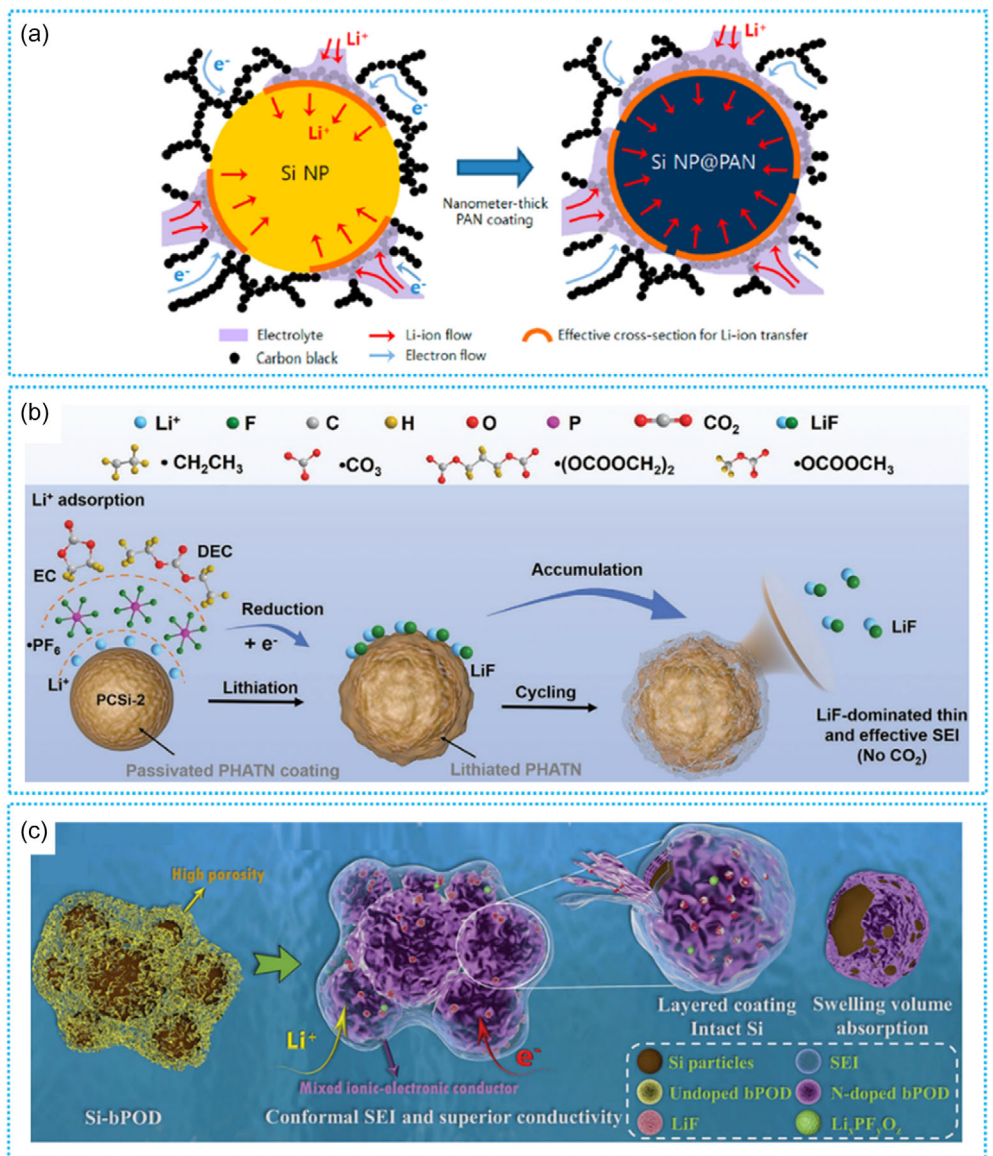


Figure 11. Schematic of three silicon and ion-conductive polymer composites. a) Nanometer-thick PAN coating leads to a larger effective cross section area for lithium-ion transfer between silicon and LE. Reproduced with permission.^[153] Copyright 2018, American Chemical Society. b) PHATN facilitates the construction of robust lithium-enriched surface coatings on silicon. Reproduced with permission.^[25] Copyright 2022, Wiley-VCH GmbH. c) bPOD layers contribute to electrode stability and SEI construction. Reproduced with permission.^[156] Copyright 2023, Wiley-VCH GmbH.

inherent in the above polymer, the Si/C-PHATN composite, Si/PPP composite, Si-bPOD composite, and LiPAA-coated Gr/Si/C composite all show improved rate capability and long-term cyclability compared to pristine silicon.

However, similar to silicon/electron-conductive polymer composites, these silicon/ion-conductive polymer composites also face the issue of containing up to 33 wt% polymer content, adversely affecting battery energy density. Therefore, further research should focus on minimizing the polymer content while maintaining good ionic conductivity.

2.3.3. Other Functions of Polymer Modifiers

Polymer modifiers can enhance the mechanical robustness of silicon anodes and alleviate their volume change. By

encapsulating silicon particles with a thin polydopamine layer, the electrode integrity is preserved, and the capacity retention of the Li⁺LEB^{Si/polydopamine} is improved.^[158] Alternatively, wrapping silicon nanoparticles with resilient PVA coatings through robust covalent bonding also enhances the mechanical stability of the Si-PVA electrode and effectively mitigates its volume expansion during lithiation.^[159] In addition, polymers like PAN can also create an “electrolyte-phobic surface,” minimizing detrimental side reactions during SEI formation and increasing ICE of nanostructured silicon anodes, offering another approach for optimizing silicon anode performance.^[160] In summary, polymer modifiers can boost the electronic and ionic conductivity of silicon anodes, improve their mechanical stability, alleviate side reactions, and ultimately enhance the rate capability and cycling stability.

In the field of silicon anode research, especially in SSBs, the exploration of polymer modifiers lags behind the study of binders, potentially due to their functional overlap with binders coupled with more intricate preparation procedures and resultant impacts on energy density and production costs. Nonetheless, polymer modifiers retain significant potential in improving the electrochemical performance of silicon anodes. To harness this potential, efforts should focus on developing advanced polymers capable of maintaining exceptional conductivity and mechanical resilience even at lower contents. Given that many modifier polymers inherently lack the adhesive capability that defines binders, ensuring interfacial compatibility between modifiers and silicon materials is crucial to prevent delamination in their composites. This can be achieved through advanced coating techniques, polymer structure modification, and composition control. Moreover, finer structural designs like 3D porous architectures and core-shell structures can still be designed to regulate the microscopic morphology of silicon anodes, better accommodating volume changes and facilitating charge transport.

2.4. Polymer Electrolytes

2.4.1. DPEs

DPEs have been investigated for use in SSBs due to their light-weight nature, good ductility, flexibility, and excellent interface compatibility. Furthermore, DPEs without any liquid solvents provide a promising opportunity to tackle safety concerns associated with LEs. The lone pair electrons of nitrogen, oxygen, or fluorine elements present in the polymer matrix of DPEs (e.g., PEO, PMMA, PVDF, P(VDF-co-HFP), and PAN) play a crucial role in facilitating ion transport through central complexation and dissociation of lithium ions. Moreover, by adjusting the degree of crystallinity and morphology of the polymer matrix, the ion mobility and transport rate can be tuned to meet the specific requirements of the intended application.^[161–166]

Significant advancements have been achieved in the development of DPEs, yet their combination with silicon anodes has not been reported very often. Liu et al. investigated the electrochemical performance of the $\text{SiO}_{1.1}\text{-Li}_{2.6}\text{Co}_{0.4}\text{N}$ composite electrode with PEO electrolyte. They discovered that adding BaTiO_3 improves the mechanical stability of the electrolyte, thereby enhancing capacity retention. However, the ionic conductivity remains low, resulting in a capacity of only 500 mAh g^{-1} .^[167] Kobayashi et al. combined SiO/graphite composite with PEO-based electrolyte and achieved reversible capacity of 1068 mAh g^{-1} with a capacity retention of 72% at the 100th cycle.^[168] Si et al. employed a PEO/LiTFSI-based DPE in the cell with carbon coated silicon (Si/C) anode dispersed on carbon paper. The ${}^{\text{Li}}\text{DPEB}^{\text{Si/C}}$ exhibited a high ICE of 77% and a steady reversible capacity of 710 mAh g^{-1} after 250 cycles at 60°C at 0.1 A g^{-1} .^[169] These initial studies involving PEO-based DPEs have validated their feasibility and effectiveness in enhancing the performance of SSB with silicon anodes. Nevertheless, challenges remain stemming from limited ionic conductivity at ambient temperatures, coupled with inadequate mechanical durability.^[81,168,169]

To address the limitations of PEO-based DPEs, recent research efforts have shifted towards designing novel polymer matrices for DPEs. He et al. devised an integrated silicon anode paired with a self-healing dynamic super molecular elastomer electrolyte (SHDSE) through in situ polymerization, whose structure and work mechanism are illustrated in Figure 12a. The SHDSE electrolyte can self-heal fully within 10 min at room temperature after being cut due to the breaking and reforming of hydrogen bonds between ester and amino groups in monomer units. Additionally, hydrogen bonding between polar solvent molecules and polymer chains enhances the mechanical elasticity of the electrolyte, ensuring good contact with the electrode during charging and discharging. Consequently, the in situ constructed ${}^{\text{Li}}\text{DPEB}^{\text{Si-SHDSE}}$ batteries establish molecular-level contacts between the electrolyte and electrode interfaces, facilitating continuous and stable lithium-ion transport, minimizing silicon particle movement, and mitigating electrode volume expansion. The ${}^{\text{Li}}\text{DPEB}^{\text{Si-SHDSE}}$ cell demonstrates 68.1% capacity retention over 500 cycles and an ICE of 99.8%, which is improved compared with the ex-situ constructed ${}^{\text{Li}}\text{DPEB}^{\text{Si-SHDSE}}$ cell.^[170]

Furthermore, Pan et al. designed an elastic solid electrolyte specifically tailored for silicon anodes, which effectively eliminates the need of SSBs for external stack pressure. This electrolyte comprises a highly solvated, soft poly-dimethyl acrylamide (DMAM) phase and a poorly solvated, rigid poly-acrylamide (AM) phase, embedded within a N-methylacetamide(NMA)-lithium bisfluorosulfonimide (LiFSI) matrix, whose molecular structure is depicted in the left of Figure 12b. By combining the stretchability of soft phase with the strength of rigid phase, the copolymer matrix exhibits a large break elongation of 1160% and a high fracture strength of 1.7 MPa. Moreover, the copolymer possesses excellent shape memory capabilities, demonstrating swift deformation recovery within just 5 min after being stretched to 450% of its original length. Additionally, the elastic electrolyte also boasts a high ionic conductivity of $2 \times 10^{-3} \text{ S cm}^{-1}$ at ambient temperature, attributed to the significant dissociation of lithium salt. When coupled with micron-sized Si anode in coin-type cells (depicted in the right of Figure 12b), the ${}^{\text{Li}}\text{DPEB}^{\text{micron-sized Si}}$ half-cell demonstrates a reversible specific capacity of $1039.7 \text{ mAh g}^{-1}$ at 0.4C and a capacity retention of 90.8% after 300 cycles, while the ${}^{\text{micron-sized Si}}\text{DPEB}^{\text{LiFePO}_4}$ full cell presents a capacity retention of 98.3% over 100 cycles.^[171]

This research highlights the ability of the elastic electrolyte to effectively manage mechanical stresses within the SSB, enabling it to operate solely on the built-in coin cell pressure. The feasibility was also verified in the pouch cell configuration, with a built-in pressure of 52 kPa originating from the cell casing. These two studies underscore the potential of an elastic polymer matrix to endow electrolytes with elasticity, self-healing ability, optimized interfaces, adhesion, and resilience. These multifunctional properties enable the electrolytes to alleviate volume expansion in silicon anodes of DPEBs, thereby enhancing their performance. Therefore, a promising advance in the field of DPEs involves developing novel multifunctional polymer matrices to improve both ionic conductivity and mechanical durability.

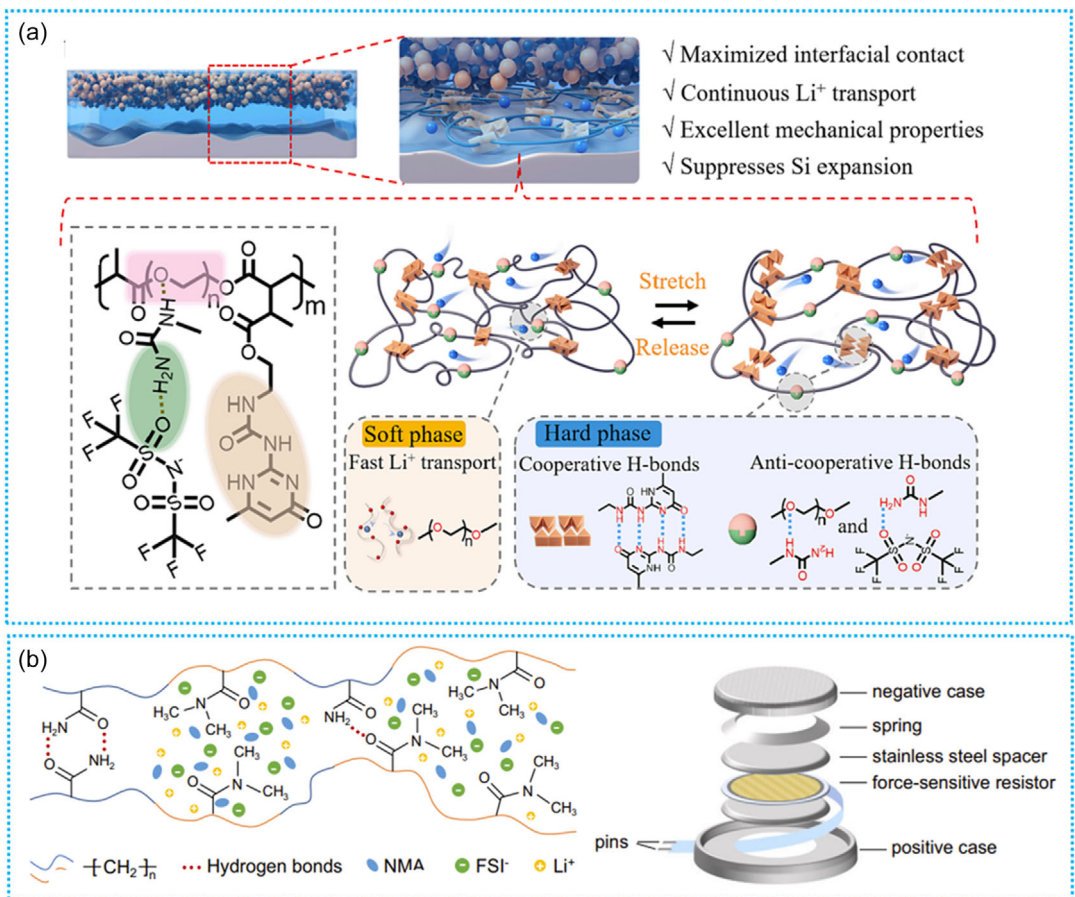


Figure 12. Schematic diagrams of two DPEs used in silicon anodes. a) Configuration of an integrated anode/polymer electrolyte for DPEB fabricated via in situ SHDSE along with molecular structure and mechanical properties of the constructed SHDSE. Reproduced with permission.^[170] Copyright 2024, Elsevier. b) Schematic of the molecular design of the elastic electrolyte and the home-made pressure sensing unit for the coin-type cell. Reproduced with permission.^[171] Copyright 2024, The Authors.

2.4.2. HEs

Incorporating inorganic SEs into organic DPEs to construct HEs can also help to address the limited ionic conductivity and inadequate mechanical durability of DPEs and further improve the performance of silicon anodes. Zhang et al. incorporated garnet fillers (LLZTO) to increase the ionic conductivity of PEO-based electrolytes and using PVDF fiber scaffolds to strengthen the composite electrolyte, as exhibited in **Figure 13a**. The composite electrolyte exhibited an ionic conductivity of $8.1 \times 10^{-5} \text{ S cm}^{-1}$ at 25 °C. When combined with a metal-organic-framework-derived carbon-hosted silicon (Si@MOF) anode, the composite electrolyte achieved conformal interfacial contact upon softening at 60 °C and maintained it throughout cycling. Consequently, the ^{Li}HEB^{Si@MOF} cell demonstrates an initial lithiation capacity of 1967 mAh g⁻¹ and maintains a reversible capacity of 1442 mAh g⁻¹ after 50 cycles.^[172] However, the authors failed to compare the properties of the PEO-based electrolyte with and without the inclusion of garnet as a filler. Therefore, the argument for an enhancement in ionic conductivity is weak, given that the interface resistance between the filler and the polymer matrix is usually very high, which hinders the transport of lithium ions. Consequently, the effectiveness of the garnet filler in

improving the ionic conductivity of DPEs remains an open question and requires further investigation to clarify its impact on the overall performance of the electrolyte system.

Similarly, Huo et al. introduced LLZTO powders into a poly(propylene carbonate) (PPC) matrix with LiTFSI to promote the dissociation of lithium salt and enhance the migration of lithium ions within the HE, achieving a conductivity of $4.2 \times 10^{-4} \text{ S cm}^{-1}$ at room temperature.^[173] The ^{Li}HEB^{Si} shows an initial discharge capacity of 2675 mAh g⁻¹ and retains 86.1% of capacity after 200 cycles. Pan et al. mixed LLZO with PVDF/PVDF-HFP + LiTFSI+propylene carbonate (PC) to facilitate the ionic conductivity and mechanical stretching strength of PVDF-based electrolytes, as showcased in **Figure 13b**. This 3D porous composite polymer electrolyte with PC plasticizer is abbreviated as 3D-PPLLP-CPEs. The constructed HE exhibited an ionic conductivity of $3.3 \times 10^{-4} \text{ S cm}^{-1}$ at room temperature, along with high mechanical strength and good interfacial contact with both NCM cathode and micro-Si@Li₃PO₄@C anode during cycling. The ^{micro-Si@Li₃PO₄@C}HEB^{NCM111} full cell delivered a capacity of 129 mAh g⁻¹ at 0.2C, maintaining 98.5% capacity retention after 100 cycles at 25 °C. Even at a higher rate of 2.0 A g⁻¹, the capacity remained 92.5 mAh g⁻¹.^[174]

To address the challenges posed by high electrolyte/electrode interface resistance in rigid ceramic electrolytes and poor

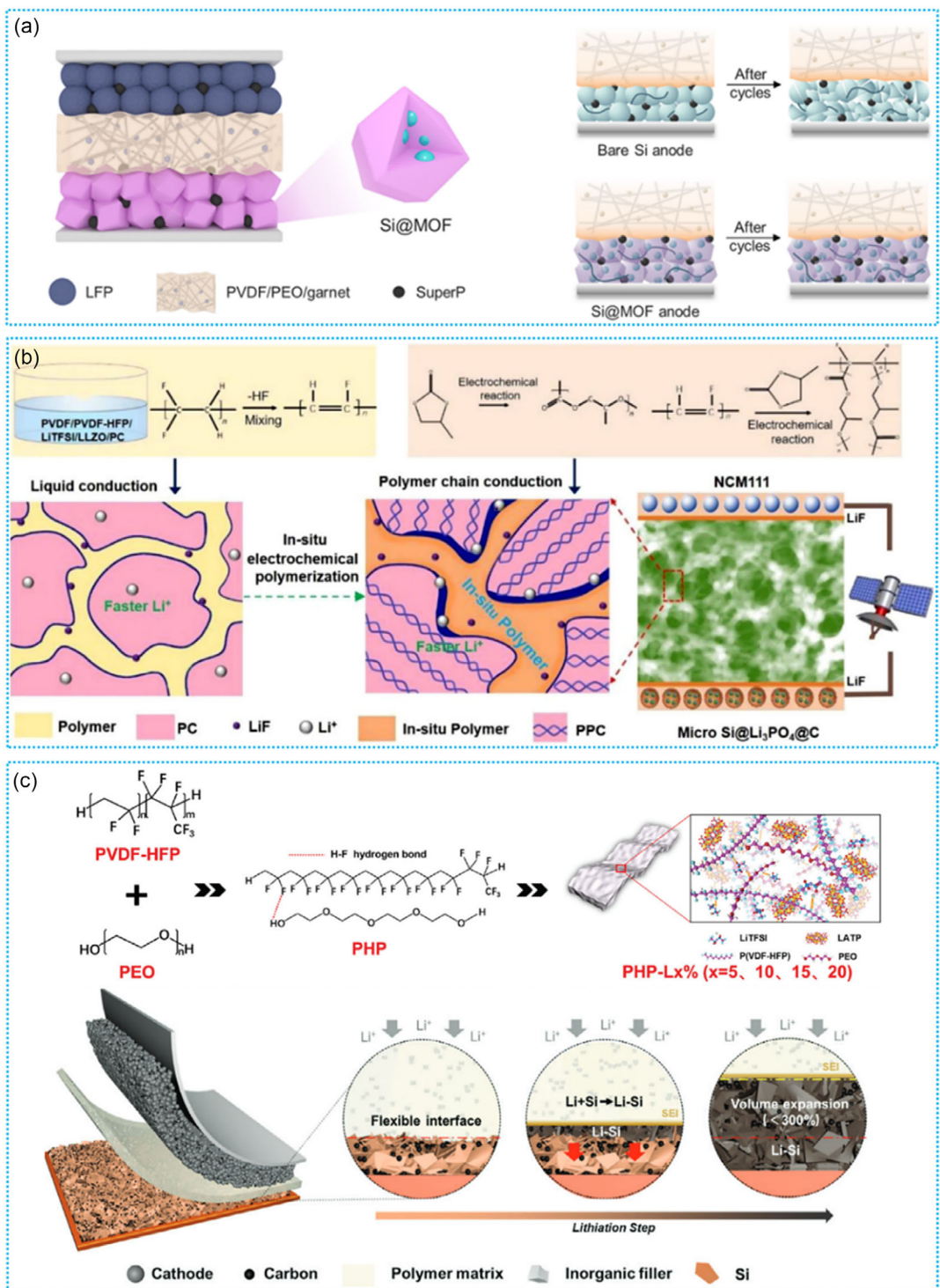


Figure 13. Schematic diagrams of HEs used in silicon anodes and their working mechanism. a) Left: schematic illustration of the Si@MOF HEB-LFP with PVDF/PEO/garnet electrolyte. Right: interfacial evolution between the PVDF/PEO/garnet electrolyte and bare silicon or the Si@MOF anode. Reproduced with permission.^[172] Copyright 2022, American Chemical Society. b) Schematic diagram of 3D-PPLP HEB. Reproduced with permission.^[174] Copyright 2021, Elsevier. c) Schematic diagram of the preparation process and structural model of the PHP-L HE and the lithiation process of silicon anode in a $\text{SiHEB}^{\text{LFP}}$. Reproduced with permission.^[175] Copyright 2024, Wiley-VCH GmbH.

ion conductivity in polymer electrolytes, both exacerbated by silicon's volume expansion, Liu et al. incorporated $\text{Li}_{1.3}\text{Al}_{0.3}\text{Ti}_{1.7}(\text{PO}_4)_3$ (LATP) into a matrix composed of PVDF-co-HFP and PEO. The resulting HE, termed PHP-L, exhibited an ionic conductivity of $1.40 \times 10^{-3} \text{ S cm}^{-1}$, coupled with remarkable tensile strength

and flexibility. This demonstrated exceptional compatibility with silicon nanosheets. The interactions between PVDF-HFP, PEO, and LATP within the HE enhance the amorphous content of the polymer matrix, facilitating faster ion transfer. The flexibility of the HE accommodated the expansion and shrinkage of the silicon

anode, thereby ensuring efficient ion transport. Furthermore, the HE solid membrane, with high tensile strength, mitigated electrode degradation and continuous interfacial growth, as demonstrated in Figure 13c. Consequently, ^{Si}HEB^{LFP} utilizing this HE demonstrated superior cycling performance compared to its performance when using LE.^[175]

Based on the presented work, it can be concluded that inorganic SE fillers, such as LLZO, LLZTO, and LATP, significantly impact the properties of HEs. To improve the performance of both HEs and silicon anode batteries, it is imperative to conduct additional research into the effects of filler morphology, content, and type on HEs. Specifically, the range of filler options could be expanded to include sulfide- or halide-based SEs. Furthermore, a deeper understanding of the interactions between the filler and polymer matrix within electrolyte systems is needed, particularly regarding the impact on aggregation structure, carrier concentration, and ion migration.

2.4.3. GEs and PPEs

GEs and PPEs incorporate liquids, solvents, or plasticizers into polymer matrices, offering intermediate states between DPEs and LEs. As the liquid content increases, the mixture properties evolve smoothly from dry polymer via plasticized polymer (solvent in polymer) and gel polymer (polymer in solvent) to liquid electrolyte.^[178] Given the continuous transition between these states, which is dependent on the additive content, distinguishing PPEs from GEs can be challenging and necessitates a case-specific distinction. Meanwhile, current research on the integration of silicon anodes with PPEs or GEs is still relatively limited. Therefore, we discuss them together here. Both GEs and PPEs exhibit improved ionic conductivity and enhanced electrolyte-electrode contact compared to DPEs, attributed to the incorporation of liquid/plasticizers that soften the polymer network.^[14]

For silicon anodes, GEs act as a mechanical cushion, alleviating the large volume change and stabilizing the interface during cycling.^[176] Bok et al. constructed a ^{Li}GEB^{Si} cell featuring silicon anode and GE composed of LE containing 2 wt% ethoxylated trimethylolpropane triacrylate (ETPTA) monomers. Benzoyl peroxide was added as a radical initiator to facilitate thermal crosslinking.^[177] The resultant GE demonstrates similar ionic conductivity as the corresponding LE, attributed to the strong interaction between lithium-ions and the nine oxygen atoms of ETPTA molecule. Furthermore, the crosslinked GE displays adequate mechanical flexibility, which mitigates the stress and strain generated during cycling, suppressing volume expansion of silicon anodes by 1.5–2 times compared to LEs. In another study, Cho et al. introduced the ethylene carbonate-based LE containing 2 wt% of polyvinyl alcohol-cyanoethyl (PVA-CN) into the cells with silicon anode. The in situ thermal gelation of the GE effectively mitigates pulverization of silicon and maintains the electrode integrity throughout repeated cycling, as illustrated in Figure 14a.^[178] The silicon anode paired with this GE remains crack-free after 50 cycles. This crack resistance is attributed to improved cohesion of the GE and the immobilizing effect of its solid skeleton network, which encapsulates the entire

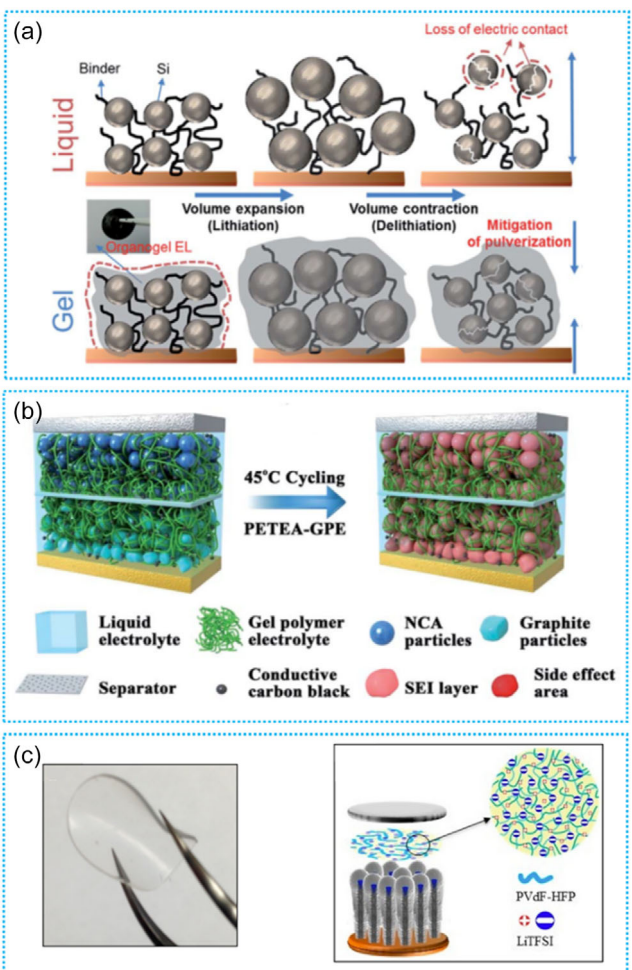


Figure 14. Schematic diagrams of typical GEs used in silicon anode-based GEBs. a) Schematic of morphological changes of silicon electrodes in LE versus GE during lithiation and delithiation. Reproduced with permission.^[178] Copyright 2016, The Royal Society of Chemistry. b) Schematic of the formation of a robust protective film on both NCA cathode and graphite-Si/C anode surface. Reproduced with permission.^[179] Copyright 2017, The Royal Society of Chemistry. c) Left: optical image of the flexible gel polymer electrolyte film with good mechanical stability that can be easily bent or stretched. Right: schematic illustration of the Si-VACNF half-cell with the GE film. Reproduced with permission.^[181] Copyright 2015, American Chemical Society.

electrode, preventing morphological deformation. Consequently, the cell with GE maintains a capacity of 2 mAh cm^{-2} at the 150th cycle with 75% retention. In contrast, the cell using LE shows a drastic capacity decline starting from the 110th cycle.

In addition to serving as a mechanical cushion, GEs can also promote the formation of a compact protective film on the surface of the silicon electrodes during cycling. This protective film helps to minimize the lithium consumption and reduce side reactions with the electrolyte. Li et al. developed a ^{graphite-Si/C}GEB^{NCA} with high energy density via in situ polymerization of 1.5 wt% pentaerythritol tetraacrylate (PETEA) in LE, which exhibits ionic conductivity of $8.46 \times 10^{-3} \text{ S cm}^{-1}$. This GE forms a robust protective film on both anode and cathode surface, as exhibited in Figure 14b, which effectively suppresses side reactions and preserves electrode integrity during cycling, leading to an improved

Table 2. Composition and performance measures for silicon anode-based batteries with different use types of polymers subdivided according to the sequence of chapters in this review. Data is as noted in the respective references.

Notation	Silicon electrode material	Separator	Binder	Mass loading [mg cm ⁻²]	Current density [mA g ⁻¹]	C-rate	ICF [%]	Total cycles	Last cycle capacity [mAh g ⁻¹]	Capacity retention [%]	Capacity after 100 cycles ^{a)}	References
$\text{Li}_{\text{LEB}^{\text{Si-MP}}}$	Si-MP	Celgard 2500	PVDF-b-PTFE	1.0	4200	1C	83	250	≈1000	72	≈1000	[31]
$\text{Li}_{\text{LEB}^{\text{Si/C}}}$	Si/natural graphite	–	PVDF-g-PAA	1.6–2.1	300	0.5C	78	50	440	88	–	[37]
$\text{Li}_{\text{LEB}^{\text{Si-NP}}}$	Si-NP	Celgard 2300	PAAl/Lys	0.65–0.85	2000	–	88	250	1008	–	≈1500	[33]
$\text{Li}_{\text{LEB}^{\text{Si-MP}}}$	Si-MP	Polyethylene	PR-PAA	1.07	600	0.2C	91	150	2271	91	≈2271	[39]
$\text{Li}_{\text{LEB}^{\text{Si-MP}}}$	Si-MP	Polypropylene	PAA-SA-borax	1.0–2.0	4000	–	93	600	1500	91	≈1500	[55]
$\text{Li}_{\text{LEB}^{\text{Si-MP}}}$	Si-MP	Asahi Kasei	SHP	0.5–0.7	400	0.1C	>80	90	≈2000	80	≈1900	[58]
$\text{Li}_{\text{LEB}^{\text{Si-MP}}}$	Si (870 nm)	Celgard 2400	SHP	0.75–1.1	360	0.1C	–	175	1360	80	≈1500	[64]
$\text{Li}_{\text{LEB}^{\text{Si-MP}}}$	Si (250 nm - 8 μm)	Celgard 2400	SHP	0.5–0.6	265	–	87	120	2407	85	≈2400	[65]
$\text{Li}_{\text{LEB}^{\text{Si-MP}}}$	Si (D50: 0.8 μm)	Celgard 2400	SHP	0.5–0.7	1790	0.5C	83	150	1300	80	≈1500	[207]
$\text{Li}_{\text{LEB}^{\text{Si/C}}}$	Si/graphitic carbon	Celgard 2400	SHP	1.2	100	–	–	100	722	83	722	[66]
$\text{Li}_{\text{LEB}^{\text{Si-NP}}}$	Si-NP	Celgard 2400	SHP	0.5–0.6	–	0.5C	70	350	1450	53	≈1800	[62]
$\text{Li}_{\text{LEB}^{\text{Si-NP}}}$	Si-NP	–	SHP	0.4–0.6	2100	0.5C	86	110	2638	74	≈2600	[61]
$\text{Li}_{\text{LEB}^{\text{Si-NP}}}$	Si-NP	Celgard 2400	SHP	1.2	4200	1C	–	250	870	86	≈1300	[67]
$\text{Li}_{\text{LEB}^{\text{Si-NP}}}$	Si-NP	Celgard 2400	SHP	0.6	–	0.2C	87	285	2591	81	≈3000	[59]
$\text{Li}_{\text{LEB}^{\text{Si-NP}}}$	Si-NP	Celgard	SHP	0.7–2.6	1790	0.5C	94	100	2312	84	2312	[109]
$\text{Li}_{\text{LEB}^{\text{Si-NP}}}$	Si-NP	Celgard 2400	SHP	1.0	1000	–	89	220	2394	94	≈2500	[68]
$\text{Li}_{\text{LEB}^{\text{Si-NP}}}$	Si-NP	Celgard 2400	SHP	0.5	–	0.2C/0.5C	82	150	2141	65	≈2300	[69]
$\text{Li}_{\text{LEB}^{\text{Si-NP}}}$	Si-NP	–	SHP	0.25–2.1	–	0.2C	83	100	≈2700	87	≈2700	[71]
$\text{Li}_{\text{LEB}^{\text{Si-NP}}}$	Si-NP	–	SHP	0.95	4000	0.3C	89	100	≈3000	97	≈3000	[72]
$\text{Li}_{\text{LEB}^{\text{Si-NP}}}$	Si-NP	–	SHP	0.5–0.6	–	0.5C	86	200	1076	41	≈1250	[73]
$\text{Li}_{\text{LEB}^{\text{Si-NP}}}$	Si-NP	Celgard 2400	PANI-based	0.2–0.35	1000	–	69	500	1137	–	≈1270	[82]
$\text{Li}_{\text{LEB}^{\text{Si-NP}}}$	Si-NP	–	PANI	0.2–0.3	6000	–	70	5000	550	90	≈400	[203]
$\text{Li}_{\text{LEB}^{\text{Si-NP}}}$	Si-NP	Whatman GF/A	PEDOT:PSS	–	500	–	86	200	1952	68	≈2150	[101]
$\text{Li}_{\text{LEB}^{\text{Si-NP}}}$	Si-NP	–	PF-based	0.22	420	0.1C	<60	650	2100	–	≈2400	[53]
$\text{Li}_{\text{LEB}^{\text{Si-Md}}}$	Si (0.5 μm)	–	b-POD	0.4–0.6	–	0.1C	89	100	2777	–	2777	[98]
$\text{Li}_{\text{LEB}^{\text{Si-NP}}}$	Si-NP	Celgard 2400	PEDOT:PSS	0.8	1000	–	>80	200	1958	71	≈2150	[91]
$\text{Li}_{\text{LEB}^{\text{Si-NP}}}$	Si-NP	Celgard 2400	PEDOT:PSS	0.6–0.8	716	0.2C	–	100	1872	–	1872	[92]
$\text{Li}_{\text{LEB}^{\text{Si-NP}}}$	Si-NP	–	PF-COONa	0.61	420	–	68	100	2521	84	2521	[95]

Table 2. Continued.

Notation	Silicon electrode material	Separator	Binder	Mass loading [mg cm ⁻²]	Current density [mA g ⁻¹]	C-rate [%]	Total cycles	Last cycle capacity [mAh g ⁻¹]	Capacity retention [%]	Capacity after 100 cycles ^{a)}	References
$\text{Li}^{\text{I}}\text{LEB}_{\text{Si-NP}}^{\text{I}}$	Si-NP	—	PPQ-COOONa	1.2	—	0.2C	—	200	1725	76	≈ 2200 [108]
mesoporous-Si SEB^{Ilin}	mesoporous Si	77.5Li ₂ S ₂₂ PS ₅	stabilized PAN	0.58	—	0.067C	45	100	490	23	490 [110]
$\text{Li}^{\text{I}}\text{LEB}_{\text{Si-NP}}^{\text{I}}$	Si-NP	Celgard 2325	starch/PEG	0.88	500	—	70	300	1100	32	≈ 1500 [120]
$\text{Li}^{\text{I}}\text{LEB}_{\text{Si-NP}}^{\text{I}}$	Si-NP	—	PEO-PEI/PEDOT:PSS	2.2	1000	—	82	500	2027	83	≈ 2600 [99]
$\text{Li}^{\text{I}}\text{LEB}_{\text{Si-NP}}^{\text{I}}$	Si-NP	—	PAA-DA/PVA	—	4000	—	83	500	1974	51	≈ 2700 [127]
$\text{Li}^{\text{I}}\text{LEB}_{\text{Si-NP}}^{\text{I}}$	Si-NP	Celgard 2400	N-P-LIPN	0.7-1.0	—	0.2C	93	100	2143	—	2143 [130]
$\text{Si}-\text{N}_x\text{SEB}^{\text{Ilin}}$	Si-NP	Li ₆ PS ₅ Cl	heat treated PAN	—	—	1C	84	200	1122	77	≈ 1300 [111]
$\text{Li}^{\text{I}}\text{LEB}_{\text{Si-NP}}^{\text{I}}$	Si-NP	Celgard 2480	PAA	0.45-0.5	—	0.1C	85	100	2920	80	2920 [133]
$\text{Li}^{\text{I}}\text{LEB}_{\text{Si-NP}}^{\text{I}}$	Si	Celgard 2325	PVAm	0.8-1	420	0.1C	200	200	2000	53	≈ 2250 [136]
$\text{Li}^{\text{I}}\text{LEB}_{\text{Si-NP}}^{\text{I}}$	Si-NP	Celgard 2500	PVA-boric acid	1.0	840	0.2C	93	500	1884	—	≈ 2600 [137]
$\text{Li}^{\text{I}}\text{LEB}_{\text{Si-NP}}^{\text{I}}$	Si-NP	—	fluorinated binder	1.1	1500	—	86	300	2000	84	≈ 2600 [138]
Polymers function as modifier											
$\text{Li}^{\text{I}}\text{LEB}_{\text{Si-NP-LCP}}^{\text{I}}$	Si-NPLCP	Celgard 2500	PAA	1.0	1000	—	76	300	1000	—	≈ 1500 [152]
$\text{Li}^{\text{I}}\text{LEB}_{\text{Si@PH-Si}}^{\text{I}}$	PPy@PH-Si	PP	CMC	—	1000	—	68	250	≈ 2000 [147]	88	≈ 2200 [147]
$\text{Li}^{\text{I}}\text{LEB}_{\text{Si@PEDOT}}^{\text{I}}$	Si@PEDOT	Glass fiber	CMC-Na	0.8	500	—	62	100	1439	—	1439 [150]
$\text{Li}^{\text{I}}\text{LEB}_{\text{Si/C-PHATN}}^{\text{I}}$	Si/C with PHATN	Celgard 2325	SA	0.9-1.1	1000	—	81	500	1130	—	≈ 1500 [25]
$\text{Li}^{\text{I}}\text{LEB}_{\text{Si@x-PAN}}^{\text{I}}$	Si@x-PAN	—	CMC	1.0	—	0.5C	86	1000	—	>75	≈ 1800 [154]
$\text{Li}^{\text{I}}\text{LEB}_{\text{Si/PPP}}^{\text{I}}$	Si/PPP	Celgard 2400	PAA	—	3000	—	78	400	1600	60	≈ 2100 [155]
$\text{Li}^{\text{I}}\text{LEB}_{\text{Si/PPP}}^{\text{I}}$	Si/PPP	Glass microfiber	PAA	1.7	500	0.5C	85	500	1438	89	≈ 1750 [208]
$\text{Li}^{\text{I}}\text{LEB}_{\text{Si-bPOD}}^{\text{I}}$	Si-bPOD	—	LiPAA	1.0	3000	—	78	800	1065	80	≈ 1750 [156]
$\text{Li}^{\text{I}}\text{LEB}_{\text{Si-PDA}}^{\text{I}}$	Si-PDA	Fiberglass	PAA	0.5-0.8	700	—	83	100	1971	66	1971 [158]
$\text{Li}^{\text{I}}\text{LEB}_{\text{Si-PVA}}^{\text{I}}$	Si-PVA	—	PAA	1.0	200	—	86	100	1526	—	1526 [159]
$\text{Li}^{\text{I}}\text{LEB}_{\text{LiPAA-Gr/SiC}}^{\text{I}}$	LiPAA-coated Gr/SiC	Polyethylene	NapAA	4.5	250	0.5C	87	500	185	82	≈ 210 [157]
$\text{Li}^{\text{I}}\text{LEB}_{\text{SiO}_1\text{-SiO}_4\text{N}}^{\text{I}}$	SiO _{1.1} Li _{2.6} Co _{0.4} N	PEO-LiTFSi-BaTiO ₃	None	—	0.5 mA cm ⁻²	—	≈ 100	30	500	—	— [167]
Polymers function as electrolyte											
$\text{Li}^{\text{I}}\text{DEB}_{\text{Si/C}}^{\text{I}}$	SiO/graphite	PEO/MEEGE + LiTFSI	PVDF	—	—	0.125C	77	100	504	72	504 [168]
$\text{Li}^{\text{I}}\text{DEB}_{\text{Si/C}}^{\text{I}}$	Si/C	PEO/LiTFSI	None	—	100	—	77	250	710	72	≈ 1000 [169]
$\text{Li}^{\text{I}}\text{DEB}_{\text{Si/SHDSE}}^{\text{I}}$	Si-NP	SHDSE	PAA	1.1	1000	—	88	500	1772	68	≈ 2400 [170]

Table 2. Continued.

Notation	Silicon electrode material	Separator	Binder	Mass loading [mg cm ⁻²]	Current density [mA g ⁻¹]	C-rate	ICE [%]	Total cycles	Last cycle capacity [mAh g ⁻¹]	Capacity retention [%]	Capacity after 100 cycles ^{a)}	References
$\text{LiDPEB}_{\text{Si-MP}}$	Si-MP	Elastic DPE	PAA	0.5–0.7	1432	0.4C	87	300	944	91	≈900	[171]
LiHEB_{Si}	Sputtered Si	PPC + LLZTO + LiTFSI	None	—	—	0.1C	68	200	2296	86	≈2350	[173]
LiHEB_{Si}	Si nanosheet	PVDF-co-HFP/PEO/LATP	None	—	0.65 mA cm ⁻²	1C	67	200	817	—	≈1700	[175]
$\text{Si@Li}_3\text{PO}_4@\text{C}$	$\text{Si@Li}_3\text{PO}_4@\text{C}$	PVDF/PVDF-co-HFP + LLZTO + LiTFSI	PVDF	—	200	0.2C	—	100	129	99	129	[174]
HEB_{NCM}	—	—	—	—	—	—	—	—	—	—	—	—
$\text{LiHEB}_{\text{Si@MOF}}$	Si@MOF	PVDF-PEO-LTZTO	None	—	200	—	72	50	1442	73	—	[172]
$\text{Si@MOF-HEB}^{\text{LFP}}$	Si@MOF	PVDF-PEO-LTZTO	None	—	34	0.2C	—	500	99	73	≈125	[172]
$\text{LiGEB}^{\text{mesop-Si}}$	Mesoporous Si	ETPTA-mediated GE	PAA + CMC	—	—	0.2C	—	100	>2000	92	>2000	[177]
$\text{LiGEB}_{\text{Si-NP}}$	Si-NP	(PVA-CN) GE	PAA + CMC	1.3	508	0.2C	87	150	1903	75	≈2100	[178]
Graphite-Si/C	Graphite-Si/C	PETEA-based GE	SBR + CMC	7.4	—	5C	—	200	1.65 Ah	81	≈1.68 Ah	[179]
GEB^{NCA}	—	—	—	—	—	—	—	—	—	—	—	—
$\text{Si-graphite GEB}^{\text{NCM}}$	Si-graphite	PVA-CN-based GE	SBR + CMC	4.4	—	—	—	300	105	75	≈127	[180]
$\text{LiGEB}_{\text{Si-VACNF}}$	Si-VACNF	PVDF-co-HFP + LiTFSI + EC/DMC	None	—	2600	—	—	100	1070	88	1070	[181]

^{a)}Approximate values (with ≈) estimated from the respective Figures of cycling data.

capacity retention of 81% after 200 cycles at a discharge rate of 5C. This outperforms the cell implementing conventional LEs, which only retain 51% of their capacity under the same conditions.^[179]

Zhao et al. fabricated a PVA-CN-based GE for $\text{Si-Gr}_{\text{GEB}}^{\text{NCM}}$ full cell via in situ gelation of a precursor solution composed of 2 wt% PVA-CN in base liquid electrolytes, where lithium difluoro(oxalato)borate additive was employed to form a stable SEI film on the anode. Besides, the robust film also prevents LiPF_6 decomposition at the cathode surface and scavenges hydrogen fluoride to form LiF, protecting the NCM cathode from the dissolution of transition metals. Consequently, the capacity retention of the $\text{Si-graphite GEB}^{\text{NCM}}$ reaches 75.4% after 300 cycles, which is significantly higher than the 45.7% retention achieved with base liquid electrolyte alone.^[180]

The aforementioned GEs were prepared through in situ reaction of ≈2% of functional monomers that were added to the LEs. While this approach is straightforward and easy to proceed, its preparation occurs within the confines of cells, rendering the process relatively intricate and challenging to control. Conversely, the ex situ method offers a flexible and independent preparation process that avoids direct interference with the electrochemical device. Li et al. adopted this kind of ex situ approach to prepare GE via a solution casting method. This involved dissolving P(VDF-co-HFP) in intermediate solvent tetrahydrofuran, and blending the solution with a LE at a certain ratio. The resulting GE exhibits an ionic conductivity of $2.2 \times 10^{-3} \text{ S cm}^{-1}$ and a cationic transference number of 0.41 along with good thermal and mechanical stability, as evidenced in Figure 14c. By sandwiching this GE film between silicon-coated vertically aligned carbon nanofibers (Si-VACNF) and a lithium foil, the $\text{LiGEB}^{\text{Si-VACNF}}$ cell delivers a capacity of $\approx 1070 \text{ mAh g}^{-1}$ at 0.67C rate with almost no capacity fade for up to 100 cycles. The good rate capability and cycling stability of the cell are attributed to the open vertical 3D nanostructure of silicon anode, which enhances GE infiltration and accommodation of silicon expansion. Furthermore, the elasticity of GEs effectively manages stress/strain in electrodes during cycling.^[181]

The current research demonstrates that GEs offer good ionic conductivity for silicon anode batteries, serve as mechanical cushions, and facilitate the formation of a protective layer on silicon anodes. However, further fundamental research is imperative to delve into the effects of in situ gel processing and the crosslinking degree on the mechanical attributes and ionic conductivity of GEs, as well as the influence of GEs with varying properties on battery performance. Functional monomers or polymer matrices of GEs can be further expanded to those enriched with specific elements such as oxygen, nitrogen, or fluorine, which facilitate stronger interactions with lithium ions. Moreover, a comprehensive understanding of the interfacial stability between GEs and silicon anodes is necessary to achieve regulatory control. Lastly, exploring GEs and PPEs prepared via ex situ methods offers a more controlled preparation process, advanced characterization capabilities, and greater flexibility in application.

In summary, polymers have been successfully utilized as electrolyte matrices in silicon anode batteries, although only a

few types have been explored and most of them, like PEO, suffer from low ionic conductivity and poor mechanical durability. To address these issues, several novel polymers featuring super-elastic, self-healing, or shape memory capabilities have been developed and enable polymer electrolytes with optimized interfaces, adhesion, and resilience, which are expected to gain more attention in the field of DPEBs, GEBs, PPEBs, and HEBs with silicon anodes.

2.5. Performance of Cells with Silicon Anode

Currently, commercial LIBs aim to utilize silicon-graphite composite anodes rather than pure silicon, leveraging the complementary advantages of both materials to enhance capacity, rate capability, and cycling stability while addressing the cost and integration limitations of pure silicon systems.^[182–185] A representative example is Tesla's 2170 battery, which integrates a silicon-graphite hybrid anode.^[186,187] Tesla is further advancing its 4680 batteries, and Build Your Dreams (BYD) is developing a new blade prismatic cell design, yet both without detectable silicon content in the anode.^[188–190] Although PVDF remains the dominant binder in commercial applications within the cathode, alternatives such as PAA, SBR, and CMC are adopted as binder in the anode of Tesla's 4680 battery and BYD's blade prismatic cell.^[188–190]

Table 2 summarizes the composition and performance characteristics of typical batteries with silicon anode, where polymers play the role of binders, modifiers, and electrolytes. The first part of Table 2 shows that binders with strong adhesion and self-healing capabilities allow silicon anodes to achieve at least 80% ICE and retain at least 80% of their original capacity after more than 100 cycles. Binders with electron and ion conductivity generally result in capacity retention close to 80%, while the ICE varies widely from below 60% to as high as 93%. Therefore, when designing conductive binders, the binding capability and the ability to mitigate volume changes should also be considered carefully, as they are crucial for enhancing the performance of silicon anodes. Furthermore, integrating SEI regulation into the binder design can improve the performance of silicon anodes, which is still short of comprehensive research in this area.

The second part of Table 2 indicates that polymer-modified silicon anodes typically reach an ICE of ≈80% and retain about 80% of their capacity after 100 cycles. While polymer modifiers mainly enhance electron and ion conductivity in silicon anodes, similar to binders, their excessive use reduces the proportion of active silicon in the anode, thereby leading to a loss in battery energy density. This may explain the relatively less research on modifiers in comparison to binders.

The third part of Table 2 reveals that current research on polymer electrolytes used in SSBs with silicon anodes primarily focuses on PEO-based electrolytes, with some attention also on PVDF-based electrolytes. Specifically, ${}^{\text{Li}}\text{DPEB}^{\text{Si-SHSE}}$ can achieve a capacity of 1772 mAh g^{-1} (based on silicon) after 500 cycles, retaining ≈70% of its initial capacity. And $\text{Si-graphiteGEB}^{\text{NCM}}$ can attain a capacity of about 100 mAh g^{-1} (based on NCM) after 300 cycles, also maintaining about 70%

capacity retention. Future research can focus on the development of electrolytes utilizing innovative elastic polymers that possess excellent ionic conductivity and mechanical durability.

Comparing the performances of different cells is challenging due to variations in loadings and current densities. In general, ref. [55] demonstrates a notable performance for ${}^{\text{Li}}\text{LEB}^{\text{Si-MP}}$ featuring a pure microsilicon anode. This cell employs a functionally crosslinked, mechanically enhanced polymer as a binder, achieving an ICE of 93% and a reversible capacity about 1500 mAh g^{-1} with a capacity retention of 91% after 600 cycles at 4000 mA g^{-1} under a mass loading of $1.0\text{--}2.0 \text{ mg cm}^{-2}$. Meanwhile, ref. [171] showcases superior performance of ${}^{\text{Li}}\text{DPEB}^{\text{Si-MP}}$, utilizing microsilicon anode and elastic DPE. This cell exhibits an ICE of 87% and a reversible capacity of 944 mAh g^{-1} at a current density of 1432 mA g^{-1} after 300 cycles, with a similar capacity retention of 91%. These two references highlight the development trends for polymers utilized in silicon anodes, emphasizing mechanical reinforcement and high elasticity.

3. Conclusion

Silicon with high specific capacity is a promising anode material for achieving high-energy-density batteries. Utilizing or fine tuning the polymers in batteries with silicon anode represents a feasible and practical approach to address its intrinsic issues and enhance battery performance. This review showcases recent literature illustrating the diverse applications of polymers in silicon anodes, serving as binders distributed throughout the entire electrode, as modifiers exclusively coating the silicon active material, and as electrolytes to separate cathode and anode. Current topic streams of interest are SHPs, conductive polymers, super elastic polymers, with a particular focus on multifunctional polymers that integrate the attributes of self-healing, conductivity, and elasticity. The surveyed literature demonstrates the growing significance of polymers in enhancing the cohesion, conductivity, mechanical properties, interface, and structural stabilities of silicon anodes, particularly with the emergence of silicon in SSBs, providing valuable insights for future research and development in this field.

Acknowledgements

The authors are very grateful for funding from the China Scholarship Council (202104910156) and the BMBF project FLiPS (03XP0261).

Open Access funding enabled and organized by Projekt DEAL.

Conflict of Interest

The authors declare no conflict of interest.

Keywords: binder · lithium-ion batteries · polymer · silicon · solid-state batteries

- [1] H. Huo, J. R. Janek, *ACS Energy Lett.* **2022**, *7*, 4005.
- [2] A. Song, W. Zhang, H. Guo, L. Dong, T. Jin, C. Shen, K. Xie, *Adv. Energy Mater.* **2023**, *13*, 2301464.
- [3] S. Poetke, S. Cangaz, F. Hippauf, S. Haufe, S. Dörfler, H. Althues, S. Kaskel, *Energy Technol.* **2023**, *11*, 2201330.
- [4] S. Cangaz, F. Hippauf, S. F. Reuter, S. Doerfler, T. Abendroth, H. Althues, S. Kaskel, *Adv. Energy Mater.* **2020**, *10*, 2001320.
- [5] C. Zhang, F. Wang, J. Han, S. Bai, J. Tan, J. Liu, F. Li, *Small Struct.* **2021**, *2*, 2100009.
- [6] X. Zuo, J. Zhu, P. Müller-Buschbaum, Y.-J. Cheng, *Nano Energy* **2017**, *31*, 113.
- [7] L. Sun, Y. Liu, R. Shao, J. Wu, R. Jiang, Z. Jin, *Energy Storage Mater.* **2022**, *46*, 482.
- [8] M. N. Obrovac, V. L. Chevrier, *Chem. Rev.* **2014**, *114*, 11444.
- [9] A. Baasner, F. Reuter, M. Seidel, A. Krause, E. Pflug, P. Härtel, S. Dörfler, T. Abendroth, H. Althues, S. Kaskel, *J. Electrochem. Soc.* **2020**, *167*, 020516.
- [10] M. Ge, C. Cao, G. M. Biesold, C. D. Sewell, S. M. Hao, J. Huang, W. Zhang, Y. Lai, Z. Lin, *Adv. Mater.* **2021**, *33*, 2004577.
- [11] T. Shen, Z. Yao, X. Xia, X. Wang, C. Gu, J. Tu, *Adv. Eng. Mater.* **2018**, *20*, 1700591.
- [12] K. Feng, M. Li, W. Liu, A. G. Kashkooli, X. Xiao, M. Cai, Z. Chen, *Small* **2018**, *14*, 1702737.
- [13] X. Zhan, M. Li, S. Li, X. Pang, F. Mao, H. Wang, Z. Sun, X. Han, B. Jiang, Y.-B. He, M. Li, Q. Zhang, L. Zhang, *Energy Storage Mater.* **2023**, *61*, 102875.
- [14] S. Sen, F. H. Richter, *Adv. Sci.* **2023**, *10*, 2303985.
- [15] C. M. Costa, E. Lizundia, S. Lanceros-Méndez, *Prog. Energy Combust. Sci.* **2020**, *79*, 100846.
- [16] A. Saal, T. Hagemann, U. S. Schubert, *Adv. Energy Mater.* **2021**, *11*, 2001984.
- [17] D. Mecerreyres, N. Casado, I. Villaluenga, M. Forsyth, *Macromolecules* **2024**, *57*, 3013.
- [18] K. Xu, X. Liu, K. Guan, Y. Yu, W. Lei, S. Zhang, Q. Jia, H. Zhang, *ChemSusChem* **2021**, *14*, 5135.
- [19] J. Li, Y. Cai, H. Wu, Z. Yu, X. Yan, Q. Zhang, T. Z. Gao, K. Liu, X. Jia, Z. Bao, *Adv. Energy Mater.* **2021**, *11*, 2003239.
- [20] J. Lopez, D. G. Mackanic, Y. Cui, Z. Bao, *Nat. Rev. Mater.* **2019**, *4*, 312.
- [21] S. Sen, E. Trevisanello, E. Niemöller, B.-X. Shi, F. J. Simon, F. H. Richter, *J. Mater. Chem. A* **2021**, *9*, 18701.
- [22] L. Sun, Y. Liu, L. J. Wang, Z. Jin, *Adv. Funct. Mater.* **2024**, *34*, 2403032.
- [23] Z. Hu, R. Zhao, J. Yang, C. Wu, Y. Bai, *Energy Storage Mater.* **2023**, *59*, 102776.
- [24] Y. Hu, Y. Qiao, Z. Xie, L. Li, M. Qu, W. Liu, G. Peng, *ACS Appl. Energy Mater.* **2021**, *4*, 9673.
- [25] Q. Wang, M. Zhu, G. Chen, N. Dudko, Y. Li, H. Liu, L. Shi, G. Wu, D. Zhang, *Adv. Mater.* **2022**, *34*, 2109658.
- [26] Y. M. Zhao, F. S. Yue, S. C. Li, Y. Zhang, Z. R. Tian, Q. Xu, S. Xin, Y. G. Guo, *InfoMat* **2021**, *3*, 460.
- [27] Y. Yang, S. Wu, Y. Zhang, C. Liu, X. Wei, D. Luo, Z. Lin, *Chem. Eng. J.* **2021**, *406*, 126807.
- [28] H. Chen, M. Ling, L. Hencz, H. Y. Ling, G. Li, Z. Lin, G. Liu, S. Zhang, *Chem. Rev.* **2018**, *118*, 8936.
- [29] W. Zhu, J. Zhou, S. Xiang, X. Bian, J. Yin, J. Jiang, L. Yang, *Front. Chem.* **2021**, *9*, 712225.
- [30] Y. Ma, J. Ma, G. Cui, *Energy Storage Mater.* **2019**, *20*, 146.
- [31] X. Wang, S. Liu, Y. Zhang, H. Wang, A. A. Aboalhassan, G. Li, G. Xu, C. Xue, J. Yu, J. Yan, B. Ding, *ACS Appl. Mater. Interfaces* **2020**, *12*, 38132.
- [32] Y. Pan, S. Ge, Z. Rashid, S. Gao, A. Erwin, V. Tsukruk, K. D. Vogiatzis, A. P. Sokolov, H. Yang, P.-F. Cao, *ACS Appl. Energy Mater.* **2020**, *3*, 3387.
- [33] S. Zhang, K. Liu, J. Xie, X. Xu, J. Tu, W. Chen, F. Chen, T. Zhu, X. Zhao, *ACS Appl. Mater. Interfaces* **2023**, *15*, 6594.
- [34] S. Chen, H. Y. Ling, H. Chen, S. Zhang, A. Du, C. Yan, *J. Power Sources* **2020**, *450*, 227671.
- [35] Z. Li, Z. Wan, X. Zeng, S. Zhang, L. Yan, J. Ji, H. Wang, Q. Ma, T. Liu, Z. Lin, M. Ling, C. Liang, *Nano Energy* **2021**, *79*, 105430.
- [36] P.-F. Cao, G. Yang, B. Li, Y. Zhang, S. Zhao, S. Zhang, A. Erwin, Z. Zhang, A. P. Sokolov, J. Nanda, *ACS Energy Lett.* **2019**, *4*, 1171.
- [37] J. I. Lee, H. Kang, K. H. Park, M. Shin, D. Hong, H. J. Cho, N. R. Kang, J. Lee, S. M. Lee, J. Y. Kim, *Small* **2016**, *12*, 3119.
- [38] W. Wang, Y. Li, Y. Wang, W. Huang, L. Lv, G. Zhu, Q. Qu, Y. Liang, W. Zheng, H. Zheng, *Electrochim. Acta* **2021**, *400*, 139442.
- [39] S. Choi, T.-W. Kwon, A. Coskun, J. W. Choi, *Science* **2017**, *357*, 279.
- [40] A. Magasinski, B. Zdryko, I. Kovalenko, B. Hertzberg, R. Burtovy, C. F. Huebner, T. F. Fuller, I. Luzinov, G. Yushin, *ACS Appl. Mater. Interfaces* **2010**, *2*, 3004.
- [41] C.-H. Jung, K.-H. Kim, S.-H. Hong, *ACS Appl. Mater. Interfaces* **2019**, *11*, 26753.
- [42] X. Shan, Z. Cao, G. Zhu, Y. Wang, Q. Qu, G. Liu, H. Zheng, *J. Mater. Chem. A* **2019**, *7*, 26029.
- [43] L. Luo, Y. Xu, H. Zhang, X. Han, H. Dong, X. Xu, C. Chen, Y. Zhang, J. Lin, *ACS Appl. Mater. Interfaces* **2016**, *8*, 8154.
- [44] J. Li, R. B. Lewis, J. R. Dahn, *Electrochem. Solid-State Lett.* **2007**, *10*, A17.
- [45] I. Kovalenko, B. Zdryko, A. Magasinski, B. Hertzberg, Z. Milicev, R. Burtovy, I. Luzinov, G. Yushin, *Science* **2011**, *334*, 75.
- [46] N. Hamzelui, M. Linhorst, G. Martin Nyenhuis, L. Haneke, G. G. Eshetu, T. Placke, M. Winter, B. M. Moerschbacher, E. Figgemeier, *Energy Technol.* **2023**, *11*, 2201239.
- [47] M. Ling, Y. Xu, H. Zhao, X. Gu, J. Qiu, S. Li, M. Wu, X. Song, C. Yan, G. Liu, *Nano Energy* **2015**, *12*, 178.
- [48] R. Kuruba, M. K. Datta, K. Damodaran, P. H. Jampani, B. Gattu, P. P. Patel, P. M. Shanthi, S. Damle, P. N. Kumta, *J. Power Sources* **2015**, *298*, 331.
- [49] Y. Gao, X. Qiu, X. Wang, A. Gu, L. Zhang, X. Chen, J. Li, Z. Yu, *ACS Sustainable Chem. Eng.* **2019**, *7*, 16274.
- [50] J. He, L. Zhang, *J. Alloys Compd.* **2018**, *763*, 228.
- [51] M. J. Jolley, T. S. Pathan, A. M. Wemyss, I. Prokes, S. Moharana, C. Wan, M. J. Loveridge, *ACS Appl. Energy Mater.* **2023**, *6*, 496.
- [52] L. Wei, C. Chen, Z. Hou, H. Wei, *Sci. Rep.* **2016**, *6*, 19583.
- [53] J. Song, M. Zhou, R. Yi, T. Xu, M. L. Gordin, D. Tang, Z. Yu, M. Regula, D. Wang, *Adv. Funct. Mater.* **2014**, *24*, 5904.
- [54] M. Jeena, J.-I. Lee, S. H. Kim, C. Kim, J.-Y. Kim, S. Park, J.-H. Ryu, *ACS Appl. Mater. Interfaces* **2014**, *6*, 18001.
- [55] W. Yan, S. Ma, Y. Dong, M. Cao, S. Chen, Y. Li, Y. Lu, L. Chen, Q. Huang, Y. Su, F. Wu, N. Li, *Energy Storage Mater.* **2024**, *73*, 103852.
- [56] D. H. Kim, H. A. Lee, Y. B. Song, J. W. Park, S.-M. Lee, Y. S. Jung, *J. Power Sources* **2019**, *426*, 143.
- [57] S. Wu, F. Di, J.-G. Zheng, H.-W. Zhao, H. Zhang, L.-X. Li, X. Geng, C.-G. Sun, H.-M. Yang, W.-M. Zhou, D.-Y. Ju, B.-G. An, *New Carbon Mater.* **2022**, *37*, 802.
- [58] C. Wang, H. Wu, Z. Chen, M. T. McDowell, Y. Cui, Z. Bao, *Nat. Chem.* **2013**, *5*, 1042.
- [59] J. Li, G. Zhang, Y. Yang, D. Yao, Z. Lei, S. Li, Y. Deng, C. Wang, *J. Power Sources* **2018**, *406*, 102.
- [60] J. Yang, L. Zhang, T. Zhang, X. Wang, Y. Gao, Q. Fang, *Electrochem. Commun.* **2018**, *87*, 22.
- [61] G. Zhang, Y. Yang, Y. Chen, J. Huang, T. Zhang, H. Zeng, C. Wang, G. Liu, Y. Deng, *Small* **2018**, *14*, 1801189.
- [62] J. Nam, E. Kim, K. K. Rajeev, Y. Kim, T.-H. Kim, *Sci. Rep.* **2020**, *10*, 14966.
- [63] Z. Liu, C. Fang, X. He, Y. Zhao, H. Xu, J. Lei, G. Liu, *ACS Appl. Mater. Interfaces* **2021**, *13*, 46518.
- [64] J. Lopez, Z. Chen, C. Wang, S. C. Andrews, Y. Cui, Z. Bao, *ACS Appl. Mater. Interfaces* **2016**, *8*, 2318.
- [65] Z. Chen, C. Wang, J. Lopez, Z. Lu, Y. Cui, Z. Bao, *Adv. Energy Mater.* **2015**, *5*, 1401826.
- [66] Y. Sun, J. Lopez, H.-W. Lee, N. Liu, G. Zheng, C.-L. Wu, J. Sun, W. Liu, J. W. Chung, Z. Bao, Y. Cui, *Adv. Mater.* **2016**, *28*, 2455.
- [67] H. Chen, Z. Wu, Z. Su, S. Chen, C. Yan, M. Al-Mamun, Y. Tang, S. Zhang, *Nano Energy* **2021**, *81*, 105654.
- [68] Z. Xu, J. Yang, T. Zhang, Y. Nuli, J. Wang, S.-I. Hirano, *Joule* **2018**, *2*, 950.
- [69] J. Nam, W. Jang, K. K. Rajeev, J.-H. Lee, Y. Kim, T.-H. Kim, *J. Power Sources* **2021**, *499*, 229968.
- [70] F. Song, Z. Li, P. Jia, M. Zhang, C. Bo, G. Feng, L. Hu, Y. Zhou, *J. Mater. Chem. A* **2019**, *7*, 13400.
- [71] J. Ryu, S. Kim, J. Kim, S. Park, S. Lee, S. Yoo, J. Kim, N.-S. Choi, J.-H. Ryu, S. Park, *Adv. Funct. Mater.* **2020**, *30*, 1908433.
- [72] X. Jiao, J. Yin, X. Xu, J. Wang, Y. Liu, S. Xiong, Q. Zhang, J. Song, *Adv. Funct. Mater.* **2021**, *31*, 2005699.
- [73] K. K. Rajeev, J. Nam, E. Kim, Y. Kim, T.-H. Kim, *Electrochim. Acta* **2020**, *364*, 137311.
- [74] M. Yamamoto, Y. Terauchi, A. Sakuda, A. Kato, M. Takahashi, *J. Power Sources* **2020**, *473*, 228595.
- [75] W. He, W. Xu, Z. Li, Z. Hu, J. Yang, G. Qin, W. Teng, T. Zhang, W. Zhang, Z. Sun, X. Yu, *Adv. Sci.* **2025**, *12*, 2407540.
- [76] M. Kim, H. Ahn, J. Choi, W. B. Kim, *Energy Technol.* **2023**, *11*, 2201321.
- [77] R. Koever, W. Zhang, L. de Biasi, S. Schweißler, A. O. Kondrakov, S. Kolling, T. Brezesinski, P. Hartmann, W. G. Zeier, J. Janek, *Energy Environ. Sci.* **2018**, *11*, 2142.
- [78] J. A. Lewis, K. A. Cavallaro, Y. Liu, M. T. McDowell, *Joule* **2022**, *6*, 1418.
- [79] T. Qin, H. Yang, Q. Li, X. Yu, H. Li, *Ind. Chem. Mater.* **2024**, *2*, 191.
- [80] H. H. AL-Refai, A. A. Ganash, M. A. Hussein, *Mater. Today Commun.* **2021**, *26*, 101935.

- [81] Y. Liu, T. Matsumura, N. Imanishi, A. Hirano, T. Ichikawa, Y. Takeda, *Electrochim. Solid-State Lett.* **2005**, *8*, A599.
- [82] C. Zhang, Q. Chen, X. Ai, X. Li, Q. Xie, Y. Cheng, H. Kong, W. Xu, L. Wang, M.-S. Wang, H. Yang, D.-L. Peng, *J. Mater. Chem. A* **2020**, *8*, 16323.
- [83] C. Eldona, N. Hanif Hawari, F. Haidar Hamid, W. Dempwolf, F. Iskandar, E. Peiner, H. Suryo Wasisto, A. Sumboja, *Chem. - Asian J.* **2022**, *17*, e202200946.
- [84] M. Kummer, J. P. Badillo, A. Schmitz, H. G. Bremer, M. Winter, C. Schulz, H. Wiggers, *J. Electrochim. Soc.* **2014**, *161*, A40.
- [85] X. He, R. Han, P. Jiang, Y. Chen, W. Liu, *Ind. Eng. Chem. Res.* **2020**, *59*, 2680.
- [86] I. İ. Avci Yayla, N. Yuca, E. Sezer, B. Ustamehmetoglu, *Energy Storage* **2022**, *4*, e338.
- [87] Y. Shi, J. Zhang, A. M. Bruck, Y. Zhang, J. Li, E. A. Stach, K. J. Takeuchi, A. C. Marschilok, E. S. Takeuchi, G. Yu, *Adv. Mater.* **2017**, *29*, 1603922.
- [88] T. M. Higgins, S.-H. Park, P. J. King, C. Zhang, N. McEvoy, N. C. Berner, D. Daly, A. Shmeliov, U. Khan, G. Duesberg, *ACS Nano* **2016**, *10*, 3702.
- [89] N. Yuca, I. Kalafat, O. S. Taskin, E. Arici, *Polym. Adv. Technol.* **2023**, *34*, 279.
- [90] S. Qi, X. Zhang, W. Lv, Y. Zhang, D. Kong, Z. Huang, Q.-H. Yang, *ACS Appl. Mater. Interfaces* **2019**, *11*, 14142.
- [91] X. Liu, Z. Xu, A. Iqbal, M. Chen, N. Ali, C. Low, R. Qi, J. Zai, X. Qian, *Nano-Micro Lett.* **2021**, *13*, 54.
- [92] N. J. Kong, M. S. Kim, J. H. Park, J. Kim, J. Jin, H.-W. Lee, S. J. Kang, *Energy Storage Mater.* **2024**, *64*, 103074.
- [93] G. Liu, S. Xun, N. Vukmirovic, X. Song, P. Olalde-Velasco, H. Zheng, V. S. Battaglia, L. Wang, W. Yang, *Adv. Mater.* **2011**, *23*, 4679.
- [94] M. Wu, X. Xiao, N. Vukmirovic, S. Xun, P. K. Das, X. Song, P. Olalde-Velasco, D. Wang, A. Z. Weber, L.-W. Wang, V. S. Battaglia, W. Yang, G. Liu, *J. Am. Chem. Soc.* **2013**, *135*, 12048.
- [95] D. Liu, Y. Zhao, R. Tan, L.-L. Tian, Y. Liu, H. Chen, F. Pan, *Nano Energy* **2017**, *36*, 206.
- [96] Z. Song, T. Zhang, L. Wang, Y. Zhao, Z. Li, M. Zhang, K. Wang, S. Xue, J. Fang, Y. Ji, F. Pan, L. Yang, *Small Methods* **2022**, *6*, 2101591.
- [97] S.-M. Kim, M. H. Kim, S. Y. Choi, J. G. Lee, J. Jang, J. B. Lee, J. H. Ryu, S. S. Hwang, J.-H. Park, K. Shin, Y. G. Kim, S. M. Oh, *Energy Environ. Sci.* **2015**, *8*, 1538.
- [98] Y. Yu, J. Zhu, K. Zeng, M. Jiang, *J. Mater. Chem. A* **2021**, *9*, 3472.
- [99] W. Zeng, L. Wang, X. Peng, T. Liu, Y. Jiang, F. Qin, L. Hu, P. K. Chu, K. Huo, Y. Zhou, *Adv. Energy Mater.* **2018**, *8*, 1702314.
- [100] X. Liu, A. Iqbal, N. Ali, R. Qi, X. Qian, *ACS Appl. Mater. Interfaces* **2020**, *12*, 19431.
- [101] X. Liu, J. Zai, A. Iqbal, M. Chen, N. Ali, R. Qi, X. Qian, *J. Colloid Interface Sci.* **2020**, *565*, 270.
- [102] S. Hu, L. Wang, T. Huang, A. Yu, *J. Power Sources* **2020**, *449*, 227472.
- [103] L. Wang, T. Liu, X. Peng, W. Zeng, Z. Jin, W. Tian, B. Gao, Y. Zhou, P. K. Chu, K. Huo, *Adv. Funct. Mater.* **2018**, *28*, 1704858.
- [104] R. Tang, L. Ma, Y. Zhang, X. Zheng, Y. Shi, X. Zeng, X. Wang, L. Wei, *ChemElectroChem* **2020**, *7*, 1992.
- [105] K. Lee, S. Lim, A. Tron, J. Mun, Y.-J. Kim, T. Yim, T.-H. Kim, *RSC Adv.* **2016**, *6*, 101622.
- [106] K. K. Rajeev, E.-S. Kim, J. Nam, S. Lee, J. Mun, T. H. Kim, *Electrochim. Acta* **2020**, *333*, 135532.
- [107] X. Yu, H. Yang, H. Meng, Y. Sun, J. Zheng, D. Ma, X. Xu, *ACS Appl. Mater. Interfaces* **2015**, *7*, 15961.
- [108] Y. Zhao, L. Yang, Y. Zuo, Z. Song, F. Liu, K. Li, F. Pan, *ACS Appl. Mater. Interfaces* **2018**, *10*, 27795.
- [109] Y. T. Malik, S.-Y. Shin, J. I. Jang, H. M. Kim, S. Cho, Y. R. Do, J.-W. Jeon, *Small* **2023**, *19*, 2206141.
- [110] T. A. Yersak, J. Shin, Z. Wang, D. Estrada, J. Whitley, S.-H. Lee, M. J. Sailor, Y. S. Meng, *ECS Electrochem. Lett.* **2015**, *4*, A33.
- [111] N. A. Dunlap, J. Kim, H. Guthery, C.-S. Jiang, I. Morrissey, C. R. Stoldt, K. H. Oh, M. Al-Jassim, S.-H. Lee, *J. Electrochim. Soc.* **2020**, *167*, 060522.
- [112] J. Tu, L. Hu, W. Wang, J. Hou, H. Zhu, S. Jiao, *J. Electrochim. Soc.* **2013**, *160*, A1916.
- [113] R. Okuno, M. Yamamoto, A. Kato, Y. Terauchi, M. Takahashi, *IOP Conf. Ser.: Mater. Sci. Eng.*, Hiroshima, Japan **2019**, 625.
- [114] N. A. Dunlap, S. Kim, J. J. Jeong, K. H. Oh, S.-H. Lee, *Solid State Ionics* **2018**, *324*, 207.
- [115] M. Rana, Y. Rudel, P. Heuer, E. Schlautmann, C. Rosenbach, M. Y. Ali, H. Wiggers, A. Bielefeld, W. G. Zeier, *ACS Energy Lett.* **2023**, *8*, 3196.
- [116] D. Cao, T. Ji, A. Singh, S. Bak, Y. Du, X. Xiao, H. Xu, J. Zhu, H. Zhu, *Adv. Energy Mater.* **2023**, *13*, 2203969.
- [117] D. Y. Oh, Y. J. Nam, K. H. Park, S. H. Jung, K. T. Kim, A. R. Ha, Y. S. Jung, *Adv. Energy Mater.* **2019**, *9*, 1802927.
- [118] Z. Osman, A. K. Arof, *Electrochim. Acta* **2003**, *48*, 993.
- [119] C.-W. Liew, S. Ramesh, *Cellulose* **2013**, *20*, 3227.
- [120] S. N. S. Hapuarachchi, K. C. Wasalathilake, J. Y. Nerkar, E. Jaatinen, A. P. O'Mullane, C. Yan, *ACS Sustainable Chem. Eng.* **2020**, *8*, 9857.
- [121] T. Nakazawa, A. Ikoma, R. Kido, K. Ueno, K. Dokko, M. Watanabe, *J. Power Sources* **2016**, *307*, 746.
- [122] Y. H. Kwon, K. Minnici, M. M. Huie, K. J. Takeuchi, E. S. Takeuchi, A. C. Marschilok, E. Reichmanis, *Chem. Mater.* **2016**, *28*, 6689.
- [123] J. Liu, Q. Zhang, T. Zhang, J.-T. Li, L. Huang, S.-G. Sun, *Adv. Funct. Mater.* **2015**, *25*, 3599.
- [124] H. Schneider, A. Garsuch, A. Panchenko, O. Gronwald, N. Janssen, P. Novák, *J. Power Sources* **2012**, *205*, 420.
- [125] K. S. Ngai, S. Ramesh, K. Ramesh, J. C. Juan, *Ionics* **2016**, *22*, 1259.
- [126] J. Gao, C. Wang, D.-W. Han, D.-M. Shin, *Chem. Sci.* **2021**, *12*, 13248.
- [127] X. Wan, C. Kang, T. Mu, J. Zhu, P. Zuo, C. Du, G. Yin, *ACS Energy Lett.* **2022**, *7*, 3572.
- [128] S. Jiang, B. Hu, Z. Shi, W. Chen, Z. Zhang, L. Zhang, *Adv. Funct. Mater.* **2020**, *30*, 1908558.
- [129] R. Zhu, S. Y. Liu, T. T. Li, D. Yang, *Chemelectrochem* **2024**, *11*, e202400326.
- [130] Z. Li, Y. Zhang, T. Liu, X. Gao, S. Li, M. Ling, C. Liang, J. Zheng, Z. Lin, *Adv. Energy Mater.* **2020**, *10*, 1903110.
- [131] Y. J. Nam, D. Y. Oh, S. H. Jung, Y. S. Jung, *J. Power Sources* **2018**, *375*, 93.
- [132] K. H. Park, Q. Bai, D. H. Kim, D. Y. Oh, Y. Zhu, Y. Mo, Y. S. Jung, *Adv. Energy Mater.* **2018**, *8*, 1800035.
- [133] P. Parikh, M. Sina, A. Banerjee, X. Wang, M. S. D'Souza, J.-M. Doux, E. A. Wu, O. Y. Trieu, Y. Gong, Q. Zhou, K. Snyder, Y. S. Meng, *Chem. Mater.* **2019**, *31*, 2535.
- [134] K. L. Browning, R. L. Sacci, M. Doucet, J. F. Browning, J. R. Kim, G. M. Veith, *ACS Appl. Mater. Interfaces* **2020**, *12*, 10018.
- [135] T. Mochizuki, S. Aoki, T. Horiba, M. Schulz-Dobrick, Z.-J. Han, S. Fukuyama, H. Oji, S. Yasuno, S. Komaba, *ACS Sustainable Chem. Eng.* **2017**, *5*, 6343.
- [136] Y. X. Wang, X. F. Yang, Y. Yuan, Z. Wang, H. Z. Zhang, X. F. Li, *Adv. Funct. Mater.* **2023**, *33*, 2301716.
- [137] Z. Cao, X. Zheng, W. Huang, Y. Wang, Q. Qu, H. Zheng, *J. Power Sources* **2020**, *463*, 228208.
- [138] D.-Y. Han, I. K. Han, H. Y. Jang, S. Kim, J. Y. Kwon, J. Park, S. Back, S. Park, J. Ryu, *Energy Storage Mater.* **2024**, *65*, 103176.
- [139] H.-C. Tao, X.-L. Yang, L.-L. Zhang, S.-B. Ni, *J. Solid State Electrochem.* **2014**, *18*, 1989.
- [140] M. Feng, J. Tian, H. Xie, Y. Kang, Z. Shan, *J. Solid State Electrochem.* **2015**, *19*, 1773.
- [141] H.-Y. Lin, C.-H. Li, D.-Y. Wang, C.-C. Chen, *Nanoscale* **2016**, *8*, 1280.
- [142] R. Huang, Y. Xie, Q. Chang, J. Xiong, S. Guan, S. Yuan, G. Jiang, *Nano* **2019**, *14*, 1950078.
- [143] C. Li, C. Liu, K. Ahmed, Z. Mutlu, Y. Yan, I. Lee, M. Ozkan, C. S. Ozkan, *RSC Adv.* **2017**, *7*, 36541.
- [144] J. Zhou, T. Qian, M. Wang, N. Xu, Q. Zhang, Q. Li, C. Yan, *ACS Appl. Mater. Interfaces* **2016**, *8*, 5358.
- [145] J. Li, J. Huang, *Chem. Commun.* **2015**, *51*, 14590.
- [146] Z. P. Guo, J. Z. Wang, H. K. Liu, S. X. Dou, *J. Power Sources* **2005**, *146*, 448.
- [147] F.-H. Du, B. Li, W. Fu, Y.-J. Xiong, K.-X. Wang, J.-S. Chen, *Adv. Mater.* **2014**, *26*, 6145.
- [148] Z. Xu, E. Zheng, Z. Xiao, H. Shao, Y. Liu, J. Wang, *Chem. Eng. J.* **2023**, *459*, 141543.
- [149] Y. Yao, N. Liu, M. T. McDowell, M. Pasta, Y. Cui, *Energy Environ. Sci.* **2012**, *5*, 7927.
- [150] S. Li, J. Huang, J. Wang, K. Han, *Mater. Lett.* **2021**, *293*, 129712.
- [151] R. Li, Y. Chen, N. Ding, Z. Li, X. Li, *J. Mater. Sci.* **2022**, *57*, 4323.
- [152] S. Pan, J. Han, Y. Wang, Z. Li, F. Chen, Y. Guo, Z. Han, K. Xiao, Z. Yu, M. Yu, S. Wu, D.-W. Wang, Q.-H. Yang, *Adv. Mater.* **2022**, *34*, 2203617.
- [153] M.-S. Song, G. Chang, D.-W. Jung, M.-S. Kwon, P. Li, J.-H. Ku, J.-M. Choi, K. Zhang, G.-R. Yi, Y. Cui, J. H. Park, *ACS Energy Lett.* **2018**, *3*, 2252.
- [154] J. H. Yoon, G. Lee, P. Li, H. Baik, G.-R. Yi, J. H. Park, *Appl. Surf. Sci.* **2022**, *571*, 151294.
- [155] Y. Chen, S. Zeng, J. Qian, Y. Wang, Y. Cao, H. Yang, X. Ai, *ACS Appl. Mater. Interfaces* **2014**, *6*, 3508.
- [156] Y. Yu, C. Yang, Y. Jiang, J. Zhu, Y. Zhao, S. Liang, K. Wang, Y. Zhou, Y. Liu, J. Zhang, M. Jiang, *Small* **2023**, *19*, 2303779.
- [157] T. B. Truong, Y.-R. Chen, G.-Y. Lin, H.-T. Lin, Y.-S. Wu, C.-C. Yang, *Electrochim. Acta* **2021**, *365*, 137387.
- [158] U. Ahuja, B. Wang, P. Hu, J. Réthoré, K. E. Aifantis, *Electrochim. Acta* **2021**, *392*, 138993.
- [159] W. Shi, H. B. Wu, J. Baucom, X. Li, S. Ma, G. Chen, Y. Lu, *ACS Appl. Mater. Interfaces* **2020**, *12*, 39127.

- [160] C. Qian, J. Zhao, Y. Sun, H. R. Lee, L. Luo, M. Makaremi, S. Mukherjee, J. Wang, C. Zu, M. Xia, C. Wang, C. V. Singh, Y. Cui, G. A. Ozin, *Nano Lett.* **2020**, *20*, 7455.
- [161] S. Ramesh, C.-W. Liew, E. Morris, R. Durairaj, *Thermochim. Acta* **2010**, *511*, 140.
- [162] H. Fan, H. Li, L.-Z. Fan, Q. Shi, *J. Power Sources* **2014**, *249*, 392.
- [163] H. Walls, J. Zhou, J. A. Yerian, P. S. Fedkiw, S. A. Khan, M. K. Stowe, G. L. Baker, *J. Power Sources* **2000**, *89*, 156.
- [164] Z. Wen, T. Itoh, T. Uno, M. Kubo, O. Yamamoto, *Solid State Ionics* **2003**, *160*, 141.
- [165] K. Vignarooban, M. Dissanayake, I. Albinsson, B.-E. Mellander, *Solid State Ionics* **2014**, *266*, 25.
- [166] J. Luo, O. Conrad, I. F. Vankelecom, *J. Mater. Chem. A* **2013**, *1*, 2238.
- [167] Y. Liu, J. Yang, N. Imanishi, A. Hirano, Y. Takeda, O. Yamamoto, *J. Power Sources* **2005**, *146*, 376.
- [168] Y. Kobayashi, S. Seki, Y. Mita, Y. Ohno, H. Miyashiro, P. Charest, A. Guerfi, K. Zaghib, *J. Power Sources* **2008**, *185*, 542.
- [169] Q. Si, M. Kawakubo, M. Matsui, T. Horiba, O. Yamamoto, Y. Takeda, N. Seki, N. Imanishi, *J. Power Sources* **2014**, *248*, 1275.
- [170] S. He, S. Huang, X. Liu, X. Zeng, H. Chen, L. Zhao, H. Noor, X. Hou, *J. Colloid Interface Sci. Sci.* **2024**, *665*, 299.
- [171] H. Pan, L. Wang, Y. Shi, C. Sheng, S. Yang, P. He, H. Zhou, *Nat. Commun.* **2024**, *15*, 2263.
- [172] L. Zhang, Y. Lin, X. Peng, M. Wu, T. Zhao, *ACS Appl. Mater. Interfaces* **2022**, *14*, 24798.
- [173] H. Huo, J. Sun, X. Meng, M. He, N. Zhao, X. Guo, *J. Power Sources* **2018**, *383*, 150.
- [174] J. Pan, H. Peng, Y. Yan, Y. Bai, J. Yang, N. Wang, S. Dou, F. Huang, *Energy Storage Mater.* **2021**, *43*, 165.
- [175] X. Z. Liu, D. Wang, X. T. Wang, D. Y. Wang, Y. Li, J. Fu, R. Zhang, Z. Y. Liu, Y. Z. Zhou, G. W. Wen, *Small* **2024**, *20*, 2309724.
- [176] E. H. Kil, K. H. Choi, H. J. Ha, S. Xu, J. A. Rogers, M. R. Kim, Y. G. Lee, K. M. Kim, K. Y. Cho, S. Y. Lee, *Adv. Mater.* **2013**, *25*, 1395.
- [177] T. Bok, S.-J. Cho, S. Choi, K.-H. Choi, H. Park, S.-Y. Lee, S. Park, *RSC Adv.* **2016**, *6*, 6960.
- [178] Y.-G. Cho, H. Park, J.-I. Lee, C. Hwang, Y. Jeon, S. Park, H.-K. Song, *J. Mater. Chem. A* **2016**, *4*, 8005.
- [179] X. Li, K. Qian, Y.-B. He, C. Liu, D. An, Y. Li, D. Zhou, Z. Lin, B. Li, Q.-H. Yang, *J. Mater. Chem. A* **2017**, *5*, 18888.
- [180] E. Zhao, S. Luo, Y. Gu, L. Yang, S.-I. Hirano, *ACS Appl. Mater. Interfaces* **2021**, *13*, 59843.
- [181] G. P. Pandey, S. A. Klankowski, Y. Li, X. S. Sun, J. Wu, R. A. Rojeski, J. Li, *ACS Appl. Mater. Interfaces* **2015**, *7*, 20909.
- [182] P. K. Singh, K. D. Kepler, A. Kumar, Y. Leng, *J. Appl. Electrochem.* **2022**, *52*, 1691.
- [183] X. Li, A. M. Colclasure, D. P. Finegan, D. Ren, Y. Shi, X. Feng, L. Cao, Y. Yang, K. Smith, *Electrochim. Acta* **2019**, *297*, 1109.
- [184] M. Choi, E. Lee, J. Sung, N. Kim, M. Ko, *Nano Res.* **2024**, *17*, 5270.
- [185] M. Gautam, G. K. Mishra, K. Bhawana, C. S. Kalwar, D. Dwivedi, A. Yadav, S. Mitra, *ACS Appl. Mater. Interfaces* **2024**, *16*, 45809.
- [186] K. Frenander, T. Thiringer, *Electrochim. Acta* **2023**, *462*, 142760.
- [187] D. Petz, V. Baran, J. Park, A. Schökel, A. Kriele, J. Rebelo Kornmeier, C. Paulmann, M. Koch, T. Nilges, P. Müller-Buschbaum, A. Senyshyn, *Batteries* **2024**, *10*, 68.
- [188] M. Ank, A. Sommer, K. Abo Gamra, J. Schöberl, M. Leeb, J. Schachtl, N. Streidel, S. Stock, M. Schreiber, P. Bilfinger, C. Allgäuer, P. Rosner, J. Hagemeister, M. Rößle, R. Daub, M. Lienkamp, *J. Electrochem. Soc.* **2023**, *170*, 120536.
- [189] L. Zhong, Y. Sun, K. Shen, F. Li, H. Liu, L. Sun, D. Xie, *Small* **2024**, *20*, 2407297.
- [190] J. Gorsch, J. Schneiders, M. Frieges, N. Kisseler, D. Klohs, H. Heimes, A. Kampker, M. Muñoz Castro, E. Siebecke, *Cell Rep. Phys. Sci.* **2025**, *6*, 102453.
- [191] W. R. Liu, M. H. Yang, H. C. Wu, S. M. Chiao, N. L. Wu, *Electrochim. Solid-State Lett.* **2005**, *8*, A100.
- [192] S. Chen, Z. Song, Y. Ji, K. Yang, J. Fang, L. Wang, Z. Wang, Y. Zhao, Y. Zhao, L. Yang, *Small Methods* **2021**, *5*, 2100839.
- [193] S. Komaba, N. Yabuuchi, T. Ozeki, Z.-J. Han, K. Shimomura, H. Yui, Y. Katayama, T. Miura, *J. Phys. Chem. C* **2012**, *116*, 1380.
- [194] D. Mazouzi, Z. Karkar, C. R. Hernandez, P. J. Manero, D. Guyomard, L. Roué, B. Lestriez, *J. Power Sources* **2015**, *280*, 533.
- [195] D. H. S. Tan, Y.-T. Chen, H. Yang, W. Bao, B. Sreenarayanan, J.-M. Doux, W. Li, B. Lu, S.-Y. Ham, B. Sayahpour, J. Scharf, E. A. Wu, G. Deysher, H. E. Han, H. J. Hah, H. Jeong, J. B. Lee, Z. Chen, Y. S. Meng, *Science* **2021**, *373*, 1494.
- [196] W. Yan, Z. Mu, Z. Wang, Y. Huang, D. Wu, P. Lu, J. Lu, J. Xu, Y. Wu, T. Ma, M. Yang, X. Zhu, Y. Xia, S. Shi, L. Chen, H. Li, F. Wu, *Nat. Energy* **2023**, *8*, 800.
- [197] T. X. Kang, J. H. Chen, Y. Cui, Z. Wang, H. L. Xu, Z. Ma, X. X. Zuo, X. Xiao, J. M. Nan, *ACS Appl. Mater. Interfaces* **2019**, *11*, 26038.
- [198] H.-K. Park, B.-S. Kong, E.-S. Oh, *Electrochim. Commun.* **2011**, *13*, 1051.
- [199] C. Chen, S. H. Lee, M. Cho, J. Kim, Y. Lee, *ACS Appl. Mater. Interfaces* **2016**, *8*, 2658.
- [200] L. Shen, L. Shen, Z. Wang, L. Chen, *ChemSusChem* **2014**, *7*, 1951.
- [201] T. A. Skotheim, *Handbook of Conducting Polymers*, CRC Press, Boca Raton **1997**.
- [202] T.-H. Le, Y. Kim, H. Yoon, *Polymers* **2017**, *9*, 150.
- [203] H. Wu, G. Yu, L. Pan, N. Liu, M. T. McDowell, Z. Bao, Y. Cui, *Nat. Commun.* **2013**, *4*, 1943.
- [204] M. N. Gueye, A. Carella, J. Faure-Vincent, R. Demadrille, J.-P. Simonato, *Prog. Mater. Sci.* **2020**, *108*, 100616.
- [205] N. Salem, M. Lavriša, Y. Abu-Lebdeh, *Energy Technol.* **2016**, *4*, 331.
- [206] R. Na, K. Minnici, G. Zhang, N. Lu, M. A. González, G. Wang, E. Reichmanis, *ACS Appl. Mater. Interfaces* **2019**, *11*, 40034.
- [207] T. Munaoka, X. Yan, J. Lopez, J. W. F. To, J. Park, J. B.-H. Tok, Y. Cui, Z. Bao, *Adv. Energy Mater.* **2018**, *8*, 1703138.
- [208] J. Zhang, S. Fan, H. Wang, J. Qian, H. Yang, X. Ai, J. Liu, *ACS Appl. Mater. Interfaces* **2019**, *11*, 13251.

Manuscript received: February 5, 2025

Revised manuscript received: March 17, 2025

Version of record online: April 14, 2025